APPLICATIONS OF HIDDEN MARKOV MODEL AND SUPPORT VECTOR MACHINE FOR STATE ESTIMATION

MD. FAYEEM BIN AZIZ

FACULTY OF ENGINEERING

UNIVERSITY OF MALAYA

KUALA LUMPUR

2014

APPLICATIONS OF HIDDEN MARKOV MODEL AND SUPPORT VECTOR MACHINE FOR STATE ESTIMATION

MD. FAYEEM BIN AZIZ

DISSERTATION SUBMITTED IN FULFILMENT OF THE REQUIREMENTS FOR THE DEGREE OF MASTER OF ENGINEERING SCIENCE

FACULTY OF ENGINEERING

UNIVERSITY OF MALAYA

KUALA LUMPUR

2014

ABSTRACT

This thesis introduces applications of support vector machine (SVM) and hidden Markov model (HMM) for signal processing and image processing. The result of the SVM classifier treated as is used as observation to the HMM and the state is estimated by probabilistic argument maximization. The probability of state is calculated by the classification outcome and the previous state. This method is tested on two case studies. The first case study is about controlling an automated wheel chair using electrooculography (EOG) traces in electroencephalograph (EEG). EOG traces originate from eyeball and eyelid movements and they are embedded in EEG signals collected from the scalp of the user at three different locations. Features extracted from the EOG traces are used to determine whether the eyes are open or closed, and whether the eyes are gazing to the right, center or left. These features are utilized as inputs to a few SVM classifiers whose outputs are regarded as observations to an HMM. The HMM determines the state of the system and generates commands for navigating the wheelchair accordingly. The second case is related to bin level classification and collection scheduling. First the exact bin location and orientation are detected using Hough line detection and angle measurement. Then the Gabor filter (GF) features are extracted from the bin opening in the image and used as inputs to an SVM classifier. The output is the exact bin locations and waste level classification, which is empty, low, full or overflow. The classes of waste level are considered as observation of HMM to estimate the interval to collection time. The system achieves 98% accuracy in estimating the wheelchair navigation command from EOG tracing in EEG signal and 100% accuracy in estimating the waste collection schedule.

ABSTRAK

Tesis ini memperkenalkan aplikasi menggunakan gabungan mesin sokongan vektor kod (SVM) dan model Markov tersembunyi (HMM) teknik untuk pemprosesan isyarat dan imej. Hasil pengelasan SVM digunakan sebagai pemerhatian kepada HMM yang hasil keadaanya dianggandari kebarangkalian maksima hujah yang diguna pakai. Kaedah ini diuji ke atas dua kes masalah anggaran. Kes pertama adalah mengerai mata menatap kawalan gerakan kerusi roda automatik menggunakan jejak EOG. Artifak electrooculography (EOG) yang dikesan adalah berasal dari bebola mata dan pergerakan kelopak mata yang dapat dilihat di dalam isyarat EEG dan direkod dari tiga lokasi yang berbeza. Ciri-ciri yang diambil dari artifak EOG digunakan untuk menentukan sama ada mata adalah terbuka atau tertutup, dan pandangan ke kanan atau kiri. Ciri-ciri ini digunakan sebagai masukan ke beberapa penjodoh SVM yang keluarannya dianggap sebagai pemerhatian untuk HMM. HMM menentukan keadaan sistem dan menjana arahan untuk memandu arah kerusi roda itu seperti yang diarahkan. Kes kedua ialah mengenai pengesanan tahap sisa pepejal di dalam tong sampah dan penjadualan untuk kutipan. Sisir dan orientasi tong sampah dikesan dengan menggunakan teknik Hough Trasnform dan ukuran sudut. Kemudian, ciri-ciri turas Gabor (GF) akan dikeluarkan dari imej tong sampah yang dalam keadaan terbuka dan digunakan sebagai masukan ke pengelas SVM. Keluaran dari SVM adalah lokasi tong sampah tersebut dan pengelasan tahap sisa sama ada dalam tahap kosong, rendah penuh atau melimpah. Kelas tahap kepenuhan sisa ini digunakan oleh HMM sebagai pemerhatian untuk menganggarkan jadual koleksi yang berkadar dengan masa. Sistem ini mencapai ketepatan 98% dalam menganggarkan pandangan mata dari isyarat EEG untuk kawalan kerusi roda dan ketepatan 100 % dalam menganggarkan jadual kutipan sisa.

Acknowledgement

Firstly I would like to thank my supervisor, Professor Dr. Hamzah bin Arof for his invaluable guidance, patience, understanding, encouragement and supervision through the course of study until the completion of this thesis.

I would also like to convey thanks to the Ministry and Faculty for providing the financial means and laboratory facilities under High Impact Research Grant Scheme (D000016-16001). Thanks also to Dr. Norrima Mokhtar for appointing me as a research assistant.

My deep heartfelt gratitude and love to my family for the unconditional support and encouragement, assistance and patience they have provided me throughout this long process.

Last but not the least I would like to express my thanks to all of my friends for their help and advices at all times. I would specially like to thank Zahid, Arafat, Shahriar, Reza, Afaz, Mahbub, Abdullah, Asrol, Amira, Adila, Roziana and Mafuja.

Table of Contents

List of Figures

List of Tables

CHAPTER 1

Introduction

1.1 Chapter Overview

Support vector machine (SVM) is a well-known binary classification method for classifying logical or numerical features of a sample in a given instant and hidden Markov model (HMM) is well used state estimation method. In this chapter a brief background study of "Eye Gaze Controlled Wheel Chair Navigation System using EEG" and "Solid Waste Bin Level Classification and Collection Scheduling" are presented. In the following chapter the problems and the proposed solutions using HMM and SVM will be stated. This is followed by the objectives of the thesis and finally, the outline of the thesis will be described.

1.2 Eye Gaze Controlled Wheel Chair Navigation System using EOG traces in EEG:

Over the years various forms of human machine interface (HMI) systems have been developed for different purposes. Recent advancement in signal processing have enabled HMI users to issue commands in the forms of voice, motion of body parts, electromyography (EMG) [1, 2], electrooculography (EOG) [3-5], electroencephalography (EEG) [6, 7] or a combination of input signals [8, 9]. HMI using voice and visual cues like hand gestures have been successfully used by people with Parkinson disease, quadriplegia, amputated or missing limbs, and motor skill disorders [5]. Those HMI systems are not as effective for patients of amyotrophic lateral sclerosis (ALS), Motor Neuron Diseases, Guillain-Barre-Syndrome or brain stem infections due to difficulties in performing voluntary muscle movement. Those most severely affected may lose all voluntary muscle control and may be completely locked in their bodies, unable to communicate in any way. They affect nearly two million

people in the United States alone, and far more around the world [1-3]. Brain or eye activity is often the only available method of unimpaired communication [4, 5]. People largely paralyzed by massive brainstem lesions can often use eye movements to answer questions [6].

EEG is an electrical brain signal recorded from the surface of the scalp using electrodes. EEG signals have been utilized by researchers from diverse fields to study epilepsy, apnea, coma, and various brain or neural functions and disorders. EEG signals have also been used to help those with disabilities translate their intentions into computer commands via a Human Machine Interface (HMI). Several useful derivatives of EEG signals such as P300 wave [7-9], mu and beta rhythms and steady-state visual evoked potentials (SSVEP) have been investigated [10-12]. Electrooculography (EOG) is the electrical signal or potential difference between retina (negative pole) and cornea (positive pole) of the eye. The induced voltage can be measured in vertical or horizontal direction using two sets of electrodes placed at outer canthi. The EOG signal can vary from 50 to 3500μV with frequency below 100Hz. The positive pulse is generated when the cornea moves towards positive electrodes and vice versa. Besides noise, EOG signals may also contain artifacts from EEG, EMG, electrocardiography (ECG), head movement, electrodes placement and luminance. Likewise, EEG signals may also contain noise and traces of other signals like EOG.

The dipolar potential of the human eye can affect EEG signal [13] for example blinking or low frequency eye movement patterns can cause a dipolar artifact in the signal [14]. The main disadvantage of EOG is obtrusive, while EEG is invasive but not obtrusive [6]. Since electrodes are connected to the scalp via a cap worn on the head, they are attached securely so that the user can concentrate on the tusks with unobstructed sight. Progress in signal processing and statistical algorithms to classify signals allows to be implemented in BCI systems for various applications.

There are two types of classifiers widely used for signal classification and they are statistical and neural network classifiers. Previous approaches on brain signal application and analysis show that the Neural Network has a good performance in classification process but lack in robustness and speed. SVM a form of neural classifier that is stable, robust and accurate. In many instances, it has been shown that it performs better than a common artificial neural network classifier like MLP. HMM is a statistical tool that can be used to model processes that involves changing in sequences. The survey on algorithms which are mostly applied in EEG analysis is presented in Table 1.1.

Table 1.1: Properties of classifiers used in BCI research from [15]

	Linear	Non Linear	Generative	Discriminant	Dynamic	Static	Regularized	Stable	Un-stable	High Dimension robust
Classifiers										
FLDA	X			X		X		X		
RFLDA	X			X		X	X	X		
Linear-SVM	X			X		X	X	X		X
RBF-SVM		X		X		X	X	X		X
Neural Networks										
MLP		X		X		X			X	
BLR NN		X		X		X			X	
ALN NN		X		X		X			X	
TDNN				X	X				X	
FIRNN		X		X	X				X	
GDNN		X		X	X				X	
Gaussian NN		X		X		X			X	
LVQ NN		X		X		X			X	
Perceptron	X			X		X		X		
RBF-NN		X		X		X			X	
PeGNC		X		X		X	X		X	
Fuzzy ARTMAP NN		X		X			X		X	
Estimators										
HMM		X		X		X			X	
IOHMM		X			X	X			X	
Bayes quadratic		X		X			X		X	
Bayes graphical network		X		X			X		X	
k-NN		X			X		X		X	
Mahalanobis distance		X			X		X		X	

1.3 Solid Waste Bin Level Classification and Collection Scheduling:

Human activities generate waste that must be managed and disposed of properly. In areas of large population, waste is a big concern and solid waste management (SWM) is an attempt to manage, re-use and reduce the amount waste materials that are growing with the increase in human population all over the world. Increasing population, growing economy, rapid urbanization and the rise in community living standard have greatly accelerated the daily rate of municipal waste production [16]. A survey on solid waste management system of different cities in developed countries shows that efficient SWM systems require skilled personnel, appropriate equipment, right infrastructure, proper maintenance and the support of the central and local government as well as the consumers [17]. Sustained development and improvement of the existing SWM system in developing countries can only be attained with financial support of the government, interest in solid waste management and increased awareness of the negative impacts of untended waste that pollutes the environment especially in overly populated areas [18, 19].

The rapid rise of population in cities and the resulting increase in waste is posing serious challenges to local authorities and solid waste management companies handling waste collection and disposal as well as tracking the movement and flow of waste [20]. A notable number of research works on SWM have been published but most of them are related to bin truck and land fill planning and management [6]. To increase the accuracy and efficiency of SWM, the use of modern tools like radio frequency identification (RFID), general packet radio systems (GPRS), global positioning systems (GPS) and geographical information systems (GIS) are recommended [21]. Common issues that are prevalent in high density residential areas like apartments and slums are improper disposal of waste, overflowing waste bins and smelly bin area due to spill. These problems could be minimized with an online monitoring system where the

garbage level in the bins is detected automatically so that the garbage can be collected before the bins overflow and the rubbish spills.

Static garbage collection is a common practice where waste is collected from bins at fixed interval, normally once or twice a week. Johansson et al, [22] studied the effectiveness of different scheduling and routing policies based on real-time bin data from several recycling stations in Malmoe, Sweden. The study indicates that dynamic garbage collection can be implemented with the use of bins equipped with level sensors to improve the collection process, and reduce operating costs and collection time as compared to static collection with fixed routes.

1.4 Problem Statement:

Electroencephalography (EEG) is a form of electrical signal recorded from the surface of the scalp using electrodes. EEG signals obtained from some positions on the scalp contain traces of EOG signals related to vertical eyelid and horizontal eyeball movements. These movements can be classified using SVM classifiers. The gaze direction itself is not directly known but traceable from the EOG artifacts recorded. It can be inferred using an HMM if the current gaze direction is known.

In the second case study, features extracted from waste bin images are used as inputs to SVM classifiers to determine the bin position and orientation as well as the waste level inside the bins. Then the garbage collection scheduling is automatically updated by an HMM based on the level of waste detected in the bins.

1.5 Thesis Objectives

The objectives of the work presented in this thesis are stated as follows.

1. To classify and estimate states of brain signal using support vector machine (SVM) and hidden Markov model (HMM) in “Eye Gaze Controlled Automated Wheel Chair Maneuver System Using EEG”.
2. To classify the waste level and estimate the collection scheduling using support vector machine (SVM) and hidden Markov model (HMM) in “Solid Waste Bin Level Classification and Collection Scheduling System.”

1.6 Thesis Outline

This thesis is divided into five chapters. Chapter two presents a literature survey on the theory and the application areas of HMM and SVM. Brief reviews on image processing techniques that are relevant to the case studies are presented in this chapter. Semiautonomous wheel chair navigation systems those use EEG and EOG signals are presented in this chapter. The chapter ends with the description of a number of works that have been reported on solid waste bin level classification.

In Chapter 3 the methodology of the proposed wheel chair system controlled by EOG traces in EEG is explained. This includes signal acquisition, feature extraction, classification, state estimation and wheel chair navigation. The results of every step are compiled in the result and discussion section of the chapter.

Chapter 4 presents the waste bin level classification and collection scheduling system. Details of the implementation of image acquisition, image preprocessing, bin detection, feature extraction, classification and state estimation steps are elaborated. The results achieved by the proposed method are compared with those of previous methods in terms of classification accuracy and execution time is presented in the last part of the chapter.

Finally in chapter five, the works are summarized and a conclusion is drawn. Possible future works are also outlined.

CHAPTER 2

Literature Survey

2.1 Chapter Overview

In this chapter a survey on the theory and applications of hidden Markov model (HMM) support vector machine (SVM) classifier is presented. Then image processing techniques that are used in the work are described. This is followed by a short review on semi-autonomous wheel chair navigation systems that have been designed and reported. Finally recent waste level classification approaches related to the second case study is introduced.

2.2 Hidden Markov Model (HMM)

An hidden Markov model (HMM) is a doubly stochastic process with an underlying stochastic process that is not observable (it is hidden), but can only be observed through another set of stochastic processes that produce the sequence of observed symbols [23]. HMM estimates the state of system based on observations and previous states. The observation is only visible part of the system where states are deterministic hidden part of the process.

The element of the model are defined as follows

- T = Length of the observation sequence
- N = Number of possible states
- M = Number of observation symbols
- S = States (S_1, S_2… S_N)
- O = Observations (O_1, O_2… O_M)
- q_t = Estimated state at time t
- v_t = Observation at time t

There are three probabilities that govern the estimation of states form the sequence of observations. The probabilities are as follows:

- Initial state distribution: $\pi_i = P(q_1 = S_i)$, The probability of S_i the initial state,
- Transition probability distribution $A = \{a_{ij}\}; a_{ij} = P(q_{t+1} = S_i \mid q_t = S_j)$, probability of current state q_t in condition of previous state q_{t-1}.
- Emission probability distribution $B = \{b_{ij}\}; b_{ij} = P(q_t = S_i \mid v_t = O_j)$, probability of current state S_t in condition of current observation O_t.

The model is denoted by the distributions as $\lambda = (A, B, \pi)$. The state is detected by maximizing the product of probabilities as shown in equation (2.1) and (2.2).

$$P(q_t \mid \lambda) = P(\pi).P(q_t \mid q_{t-1}).P(q_t \mid v_t) \tag{2.1}$$

$$q_t = \arg\max(P(q_t \mid \lambda)) \tag{2.2}$$

Where, $P(q_t|\lambda)$ is the probability of the state q at time t for a given model λ. The distribution of probabilities between states and observations are shown in Figure 2.1. In the figure *i,j,k,l* are the instances of states and *a,b,c,d* are the instances of the observations.

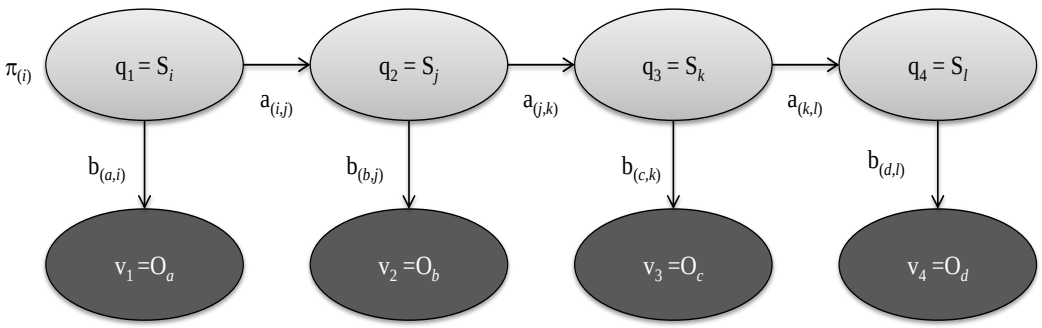

Figure 2.1: Probity distribution of hidden Markov model.

2.2.1 Basic Three Problems of Hidden Markov Model (HMM)

Computation of the probability distributions has three basic problems in real time implementation of HMM in state estimation [23]. The basic problems are:

Evaluation problem: Measure the degree of matching between a given observation sequence ($V = \{v_1, v_2 \cdots v_t\}$) and the model λ, that matching score presents how well the given model matches a given observation sequence. This problem denotes to $P(V|\lambda)$.

Decoding problem: Calculate the most likely sequence of hidden states q_i from a model $\lambda=(A,B,\pi)$ and an observed sequence $V=v_1,v_2,\ldots,v_T$.

Learning problem: Determine HMM parameters $\lambda'=(A',B',\pi')$ that best fit for training observation sequences $V = \{v_1, v_2 \cdots v_t\}$ and general structure of HMM (numbers of hidden and visible states). This is the problem of model parameters A, B and π optimization to A', B' and π' so as best describe how a given observation sequence comes about.

2.2.2 Solution of the Basic Problems

Solution of Evaluation Problem: This problem can be considered as the scoring problem of the model. The aim is to calculate the probability of the observation sequence ($V = \{v_1, v_2 \cdots v_t\}$) in condition with the given model $\lambda=(A,B,\pi)$ i.e. $P(V|\lambda)$. This problem was solved by forward-backward procedure [24, 25]. Forward variable $\alpha_t(i)$ is defined as the joint probability of v_1, v_2, v_3 ... v_t and state $q_t = S_i$ with condition of given λ. The evaluation score can be calculated from the forward variable as;

$$P(O|\lambda) = \sum_{i=1}^{N} \alpha_T(i) \tag{2.3}$$

$$\text{where } \alpha_t(i) = P(v_1 v_2 \cdots v_t, q_t = S_i \mid \lambda) \tag{2.4}$$

The backward variable $\beta_t(i)$ is defined as the probability of the partial observation sequence from $t+1$ to the end, given state Si at time t and the model λ.

$$\beta_t(i) = P(v_{t+1} v_{t+2} \cdots v_t \mid q_t = S_i, \lambda) \tag{2.5}$$

Solution of decoding problem: This problem is to find the optimal state sequence for a given observation and model can be solved in several possible ways. That means there are several possible optimal stare sequences. One well used method to solve this problem is Viterbi Algorithm [26, 27]. To find the best state sequence $Q = \{q_1, q_2 \cdots q_t\}$, for given observation sequence $V = \{v_1, v_2 \cdots v_t\}$, the best suit score can be defined as;

$$\delta_t(i) = \max_{q_1, q_2, \cdots, q_{t-1}} P(q_1 q_2 \cdots q_t = S_i, v_1 v_2 \cdots v_t \mid \lambda) \tag{2.6}$$

Where, $\delta_t(i)$ is the best score (highest probability) along a single path, at time t, which accounts for the first t observations and ends in state S_i. By induction we have:

$$\delta_{t+1}(j) = \left[\max_i \delta_t(i) a_{ij} \right] \cdot b_j(O_{t+1}) \tag{2.7}$$

The maximization of δ_t needed to be tracked to find the maximum δ_{t+1}.

Solution of learning problem: This problem is to solve the optimized parameter of the model λ. There is no conventional or deterministic method to analytically solve the problem. Initially the values of A, B and π can be assumed any values that follow the constrains. The parameters can optimized by likelihood theory by maximizing the probabilities of given training observation sequence and corresponding states.

2.3 Applications of HMM

HMM is a well-recognized tool of speech recognition [28, 29] and hand writing recognition [30, 31]. The system is also used in biomedical computational problems [32] and statistical analysis [33].

Yann et al. [34] introduced a navigation system for disable people using HMM. In this system the user can select destination from a graphical user interface (GUI). The system calculates the direction of the wheel chair movement by decoding the states from the choice of route. Morere et. al, [35] propose an intelligent navigation route selection system for disable people using HMM. The intelligent system relies on a modification of the most frequently used routes and assists the user when navigating by suggesting the next movement when the route has been recognized.

Ren et al. [36] introduced a HMM based map-matching technique for wheelchair navigation. The map-matching method employs the Viterbi algorithm to estimate the correct sidewalk segments as hidden states in a HMM in order to match GPS trajectory on the corresponding segment sequence.

Bartolein et al. [37] presented easy system of wheelchair control for severely disabled users. The gaze of the person is used to estimate the intended motion direction. This method produces state queue only from relevant gaze behavior.

In image processing HMM is used mainly for sequencial pattern recognition like hand writing and facial expression recognition. Anand et al. [38] presented a HMM-Based face recognition system along with singular value decomposition (SVD) Coefficients. Observation vectors are generated by dividing each face image into overlapping blocks and SVD coefficients acts as a base for constructing the observation sequence. The system decodes seven state of HMM from the observation through quantization process.

Samanta et al. [39] developed a handwriting recognition method using non-homogeneous HMM. The observations are extracted by Von Mises distribution and Gaussian distribution. In this method HMM parameter smoothing is applied avoid possible over-fitting and poor generalization.

2.4 Support Vector Machine (SVM)

In the field of machine learning and pattern classification support vector machine (SVM) is one of the commonly used neural classifier [40, 41].

SVM transform linear data in a nonlinear space using transfer functions. The idea is to use a mapping function that transform the data in to a linearly separable feature space from nonlinear. Kernel functions are used to transform the data in linear feature space from nonlinear attribute. The performance of the SVM largely depends on the adaption of the Kernel in the feature space. SVM has a learning theory that automatically optimizes the separating hyperplane.

Support vector machine is a kind of classifier developed on statistical learning theory. For a statistical dataset it set a decision function that split the data in two classes. Physically the decision function can be shown as a plane between the two classes. That plane is known as hyperplane. That decision function comes up with a two parameters *w* and *b*. *w* is the distant parameter and *b* is the bias (Figure 2.2). Given a training data set $T = \{(x_1, y_1), (x_2, y_2), \cdots, (x_l, y_l)\}, x_i \epsilon R^n, y_i \epsilon \{-1, +1\}, i = 1,2, \cdots, l$. If it is linearly separable, then there exist (*w*, *b*) let the following inequality tenable.

$$\begin{cases} (w \cdot x_i) + b \geq 0 & y_i = +1 \\ (w \cdot x_i) + b \leq 0 & y_i = -1 \end{cases} \tag{2.8}$$

The distance between this two parallel hyperplanes is $2/(||w||)^2$. It is reasonable to adopt the maximum margin criterion, so the above classification problem is equivalent to the primal optimization problem as;

$$\min_{w,b} \frac{1}{2}\|w\|^2 \tag{2.9}$$

$$s.t. y_i\left((w\cdot x_i)+b\right)\geq 0, i=1,2,\cdots l. \tag{2.10}$$

From the optimal solution (w^*, b^*) of equation (2.9), we obtain the optimal classification boundary $(w^*\cdot x) + b^* = 0$, and the decision function $f(x) = sgn((w^*\cdot x) + b^*)$. The data nearest to the optimal boundary are called support vectors. The result of the decision function for support vectors is 0.

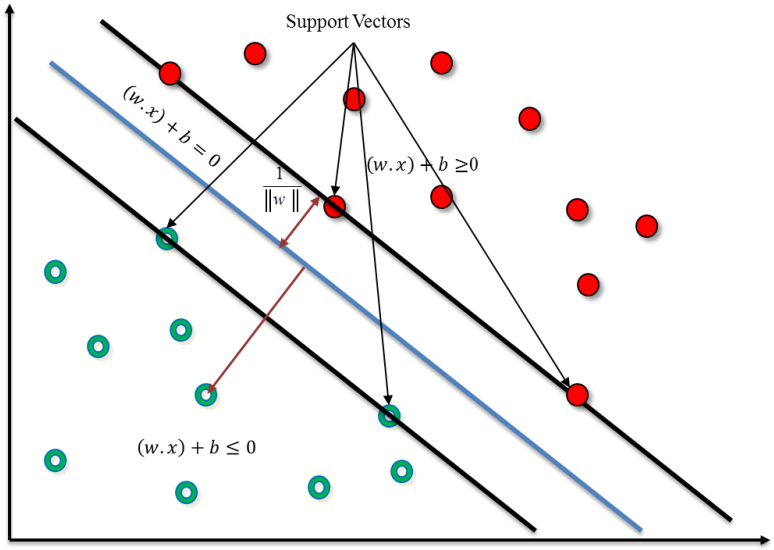

Figure 2.2: Support vector machine.

In practical, data are likely to be corrupted by noise, and then linear separable problems become almost inseparable. Also, we need think about the robust and generation performance of the method. A commonly used technique is using penalty parameters to allow misclassification. A negative variable called "slack variable" is introduced with the optimization problem mentioned equation (2.11).

$$\min_{w,b} \frac{1}{2}\|w\|^2 + C\sum^{l}\xi_i, \tag{2.11}$$

$$s.t.\ y_i\left((w\cdot x_i)+b\right)\geq -\xi_{i,}, \xi_i \geq 0, i=1,2,\cdots l.$$

Where, ξ_i is the slack variable. To solve the optimization problem equation (2.11) can be converted to the following Lagrangian dual problem:

$$\min_{w,b} \frac{1}{2}\sum_{i=1}^{l}\sum_{j=1}^{l} y_i y_j \alpha_i \alpha_j \left(x_i x_j\right) - \sum_{i=1}^{l}\alpha_i$$

$$s.t. \sum_{i=1}^{l} y_i \alpha_i = 0, 0 \le \alpha_i \le C, i = 1,2,\cdots l. \tag{2.12}$$

From the solution of equation (2.12)) we can construct the decision function:

$$f(x) = \operatorname{sgn}\left(\sum_{i=1}^{l} y_i \alpha_i (x_i \cdot x) + b\right) \tag{2.13}$$

This is the basic linear support vector machine [42]. This basic decision function makes a linear hyperplane on the feature space.

The aim of Kernel function is to build a nonlinear hyperplane that can give best classification result. Using the Kernel function the decision rule becomes

$$f(x) = \operatorname{sgn}\left(\sum_{i=1}^{l} y_i \alpha_i k(x_i \cdot x) + b\right) \tag{2.14}$$

Where, $k(x_i \cdot x) = (\varphi(x_i) \cdot \varphi(x))$ is the Kernel function. This is the nonlinear SVM [43]. This mapped data into a higher feature space including nonlinear features, then construct a hyperplane in that space so all other equations are the same. The learning model transforms the optimization into Kernel form.

$$\min_{w,b} \frac{1}{2}\sum_{i=1}^{l}\sum_{j=1}^{l} y_i y_j \alpha_i \alpha_j k\left(x_i x_j\right) - \sum_{i=1}^{l}\alpha_i$$

$$s.t. \sum_{i=1}^{l} y_i \alpha_i = 0, 0 \le \alpha_i \le C, i = 1,2,\cdots l. \tag{2.15}$$

Frequently used transfer functions include:

- Linear Kernel: $(x \cdot x') = (x \cdot x')$. (This Kernel is for the basic linear SVM)
- Polynomial Kernel: $k(x \cdot x') = \big((x \cdot x') + c\big)^d, c \geq 0.$

d is the degree of the polynomial function

- Radial basis function (RBF) Kernel: $k(x \cdot x') = e^{-\frac{||x-x'||}{\sigma^2}}$.

2.5 Applications of the SVM

For signal classification showed that SVM has been reported to show a more stable and robust performance than other neural classifiers [15, 44]. This is also true for image processing [45-47].

Xu et, al. [48] proposed a new method to reduce the number of support vectors to speed up SVM decision for Online EEG processing in motor imagery signal classification. The method first obtains all the support vectors by classical SVM. Then, γ-index that measures the average distance between each support vector and its nearest neighbors is evaluated. Next, the support vector with smallest γ-index is selected. And then iteratively re-weight γ-index and select only a few support vectors to represent all the support vectors.

Lin [49] presented an approach that identified the genre of songs played based on EEG signal classification of the listener using SVM. That system recorded a 92.73 % classification rate based on 60 features derived from EEG components in a window of one second.

Rebsamen et al. [50] presented a brain controlled wheelchair (BCW) which is based on a slow but safe P300 signal. To circumvent the problem caused by the low information rate of the EEG signal, a motion guidance strategy providing safe and efficient control without complex sensors or sensor processing is proposed in this thesis. The action of movement was detected from P-300 brainwave by SVM classification.

Jianchao Yang et al. [51] presented a spatial pyramid matching (SPM) Kernel for image classification in SVM. In this thesis an extension of the SPM method is developed generalizing vector quantization to sparse coding followed by multi-scale spatial max pooling, and propose a linear SPM Kernel based on SIFT sparse codes.

Belongie et al. [52] introduced an approach of measuring similarity between shapes and exploit it for object recognition using SVM. Features from reference points are extracted to match between two shapes. The contexts of the feature points have similarity than other points in image frame. Following this phenomenon the system detects a shape similar to a given template.

2.6 Image Processing Techniques

2.6.1 Canny Edge Detection

The edges from the gray converted image were extracted before line detection. In this method canny edge detection technique was used to find the edges. At first canny edge detector smooth the image to eliminate and noise and then finds the image gradient to highlight regions with high spatial derivatives. The algorithm then tracks along these regions and suppresses any pixel that is not at the maximum (nonmaximum suppression). The gradient array is reduced by hysteresis analysis. Two thresholds are used in hysteresis. If the magnitude of any pixel is found below than the first threshold then the pixel value is set to zero (made a nonedge), if the magnitude is found above the high threshold then it is made an edge and if the magnitude is between the two thresholds then it is set to zero unless there is a path from this pixel to a pixel with a gradient above second threshold [53].

2.6.2 Hough Transform

Hough transform is an automated digital image analysis method to detect arbitrary shapes. This transform detect parameters of shapes from the boundary points in image.

The simplest Hough transform application is line detection. A line can be defined by two parameters ρ and θ as equation (2.16).

$$y = \left(-\frac{\cos\theta}{\sin\theta}\right)x + \left(\frac{\rho}{\sin\theta}\right) \tag{2.16}$$

ρ is the distance of the line from the reference point and θ is the angel of the vector orthogonal to the line from reference point. The line parameters are shown in Figure 2.3.

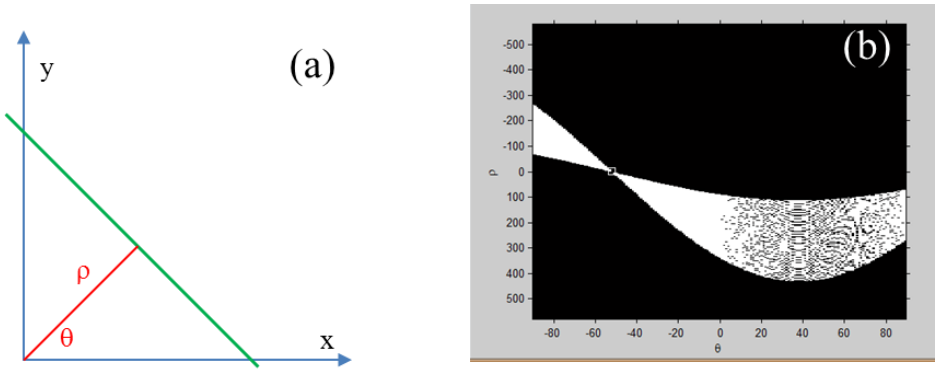

Figure 2.3: (a) Line parameters of Hough transform, (b) ρ–θ plot of Hough transform.

Each and every point in an image has corresponding ρ values for θ value from 0 to 2π. The plot of ρ against θ (Figure 2.3(b)) shows the curve of ρ values of all corresponding pixel positions of ones. The high intensity point on the plot shows the presence of pixels on same line. Selecting the picks on ρ and θ plot the parameters of a line can be calculated. The line coordinates can be calculated back from the equation (2.17).

$$x\cos\theta + y\sin\theta = \rho \tag{2.17}$$

2.7 Electroencephalography (EEG)

BCI acquire and analyze neural signals to create a communication channel directly between the brain and the computer [54]. There are several methods of recording brain

signals, such as: electroencephalography (EEG), magnetic resonance imaging (MRI) or magneto encephalography (MEG). EEG provides high temporal resolution and is comparatively easy to apply. The conventional international 10/20 system is used in EEG acquisition (Figure 2.4 (a)). The reference points in Figure 2.4(a) are the nasion and inion. The skull perimeters are measured in the transverse and median planes. Electrode locations are determined by dividing these perimeters into 10% and 20% intervals from the nasion and inion points. Three other electrodes are placed on each side, equidistant from the neighboring points as shown in Figure 2.4 (b). In this system, the electrodes are placed over the skull with a cap. A conductive gel (or fluid) is used to make contact between the skin and the electrode. Several approaches have been done to make the acquisition system more user-friendly. These include: dry contact [55], textile electrodes [56] or Emotive EPOC Interface [57]. The dipolar potential of the human eye can have a great impact on the EEG signal [13].

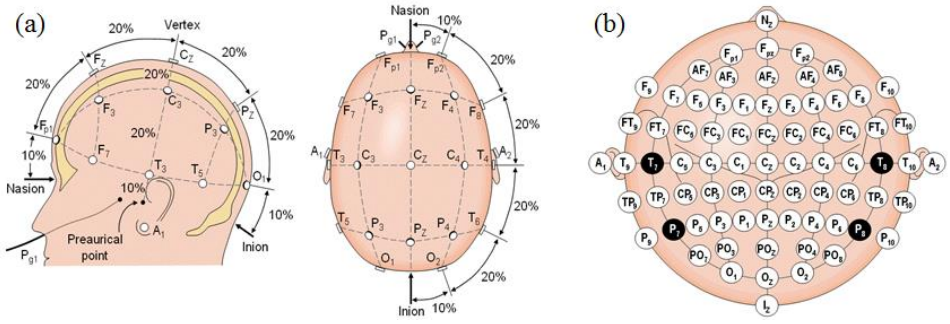

Figure 2.4: (a) International 10/20 EEG acquisition system, (b) Electrode position over head in international 10/20 system [58].

2.8 Wheel Chair Navigation Using EEG

Neuromuscular disorders affect nerves that control voluntary muscles [59, 60]. When the neurons got affected, communication between the nervous system and the muscles deteriorates thereby weakening the muscles progressively [61, 62]. People with severe motor disabilities can still maintain an acceptable quality of life with the use of HMIs that do not take signals that require muscle control as inputs. A semi-

autonomous wheelchair is an example of HMI where the user interacts with the system to navigate indoor and outdoor. Examples of semi-autonomous wheelchairs with different levels of manual assistance are listed in Table 2.1.

Table 2.1: Examples of semi-autonomous wheelchair.

HMI System	Navigation Type	Control Method	Safety Sensors	Specialty
Nav-Chair [63, 64]	Semi-Autonomous	Joystick	Ultrasonic Sensor	Avoid Obstacle
Berman Autonomous [65]	Semi-Autonomous	Joystick	Sonar Sensor	Avoid Hazard
SENARIO [66]	Semi and Full Autonomous	Voice and Goal to goal	Multiple types of sensor	Control without hand
OMNI [67]	Semi/Full Autonomous	Joy Stick and Goal to goal	Multiple types of sensor	Can be run in high or low level autonomous navigation
MAid [68]	Semi-Autonomous	Joystick	Motion Sensor	Crowed Avoidance
Wheesly [69]	Semi-Autonomous	EOG	Proximity and sonar sensor	Command system can change by the need of user
VAHM [70]	Semi/Full Autonomous	Joy Stick and Goal to goal	Ultrasonic Sensor	Combination of High and Low level autonomous navigation
Smart Wheel Chair [71, 72]	Semi-Autonomous	EEG, P-300 wave	No sensors	Run by mental tusk
BIDIM-EOG [73]	Semi-Autonomous	EOG	No sensors	Fully controlled by eye movement

Assistive robotics using EEG have been commercialized to aid human with debilitating disability ability [74]. Examples of BCI designed using EEG for this pupose are peoplebot [75], iRobot [76], robotino [77]. Several researches have been conducted by the rehabilitation engineers to develop intelligent wheel controlled by EEG or derivative of EEG for mobility assistance like NavChair [63, 64] , Berman Autonomous Wheelchair [65].

Millan et, al. [78] and Rebsamen et, al. [72] proposed methods without the mode shifting for semiautonomous wheelchair. Those systems are based on P300. The system

flashes predefined target destinations several times in a random order. The target is selected by largest P300 stimuli of the user. Then, the intelligent wheelchair reaches the selected target autonomously.

2.9 Electrooculography (EOG)

EOG is the system to measure the potential of corneo-retinal system. Several electrodes are placed around the eye. The conventional arrangement of the electrodes for obtaining an EOG signal is shown in Figure 2.5. The electrodes are made of Ag-AgCl. Two electrodes are placed to the left and to the right of the outer canthus of the eye to detect horizontal movement. Two additional electrodes are placed above and below of the eye to detect vertical movement. Another electrode is connected to the forehead of the subject (or ear) to serve as a ground. Since the signal amplitude is very low, it is passed through differential amplifiers with high gain [73, 79-81]. The voltage difference of EOG varies from 50 to 3500 μV with a frequency from DC to 100Hz. There is a nearly linear relationship between changes in the potential difference (voltage) and gaze angle. This is approximately 20 μV for each change of gaze. Two of the most successful EOG projects are integral system for assisted mobility (SIAMO) [82, 83] and Eagle eye [81] which involved rehabilitation of handicapped people.

Figure 2.5: Conventional EOG electrode assembly [81].

2.10 Wheel Chair Navigation Using EOG:

Among various types of bio signal used for wheel chair navigation EOG is found to be easy to acquire and analyse like EEG.

Barea et. Al, [73, 80, 84] developed a navigation system consists of a standard electric wheelchair with an on-board computer, sensors and a graphic user interface (GUI) run by the computer. They have introduced a model named BiDiM-EOG which controls the cursor of the GUI. The user can convey command by clicking direction option on the GUI.

Yathunanthan et. Al, [85] introduced a system to detect eye movement by processing EOG signal, and associates the eye movement to motion commands of the wheelchair such as forward, reverse, left and right. That system detects the peaks of the EOG to identify eye movement directions that is interpreted to movement command of the wheel chair. A 99% accurate classification rate has been by this experiment. Wijesoma et. al. [86] and Champaty et. al, [87] developed a mobile assistive platform that can be controlled by eye using the peaks in EOG. Boquete et. al, [88] also used EOG as media of navigation command in eye movement guided wheel chair navigation. That system detects and classifies the eye movement using artificial neural network. Noor et. al, [89] applied fuzzy logic to interpret wheel chair navigation commands from EOG peaks.

Hashimoto et. al, [90] developed the command conveying system using both EOG and EMG signals. Based on the biopotential signals, the interface recognizes the operator's gestures, such as closing the jaw, wrinkling the forehead, and looking towards left and right. By combining these gestures, the operator controls linear and turning motions, velocity, and the steering angle of the wheelchair.

Wei et. al, [91] presented a combined system using EOG and EMG to classify human facial movement based on multi-channel forehead bio-signals. Five face

movements form three face regions: forehead, eye and jaw are selected and classified in back propagation artificial neural networks (BPANN) by using a combination of transient and steady features from EMG and EOG waveforms. The identified face movements are subsequently employed to generate five control commands for controlling a simulated Intelligent Wheelchair.

2.11 Solid Waste Bin Level Classification and Collection Scheduling

Bin level is very important information for the collection and disposal of wastes. Bin level detection has been studied by several researchers for last five years. Early researchers used different kinds of sensors to detect the bin. Due to the cost ineffectiveness and workload, recent researches are focused on image processing techniques in this regards.

2.11.1 Sensor Based Methods

Garbage bin level detection has been proposed and studied as a means to improve the collection and disposal of wastes in the last five years. In one pilot study, infrared LED level sensors equipped with wireless communication system were installed in 3300 garbage bins in Sweden [22]. In each bin, four sensors were installed at different height. The garbage level is detected by the highest sensor obstructed by the wastes. Other types of sensors proposed by researchers are capacitive moisture sensor [92], point-level capacitive sensor [93] and optical sensor [94]. However, the cost of installation and regular cleaning of the sensors lead many to believe that using sensors for bin level detection is impractical. Skilled personnel are required to clean and or troubleshoot defective sensors and mountings regularly. This process the process is tedious and time consuming. Moreover, some sensors are only suitable to be used in certain conditions. For example, capacitive sensors those are sensitive to humidity, work well for volume measurements during rainy season.

2.11.2 Image Processing Based Methods

An automated bin collection system based on a combination of image processing and digital distance sensors was developed by a team of researchers from Politecnico di Milano and the Shanghai Jiao Tong University [11]. A low cost image acquisition system and distance sensors were used to detect changes in waste level in the bins. The difference between two consecutive frames of acquired images and the height of the bin level measured by the distance sensors were monitored in real time. In another work, Vicentini et al. employed a similar image difference technique to detect both change and height of the waste level in a bin by subtracting the previous frame from the current frame [12]. An intelligent real time image processing method using a motion sensor and camera was introduced by Zhu et al. [13]. The closing and opening of bin was detected by motion sensor and images of the bin were captured by a camera mounted over it. The level of waste in the bin was determined by comparing two consecutive images. The drawback of methods that rely on image difference is the need to always capture exactly the same area or objects in consecutive image frames. Thus, it is important to ensure the camera position is fixed relative to the bin opening area at all time. A little jitter, shift or rotation to the mounting or the camera itself results in erroneous classification. This stringent requirement is impractical in real time applications. To neutralize this deficiency, advanced statistical learning theories and image processing techniques were used in subsequent works that adopted image difference technique [10].

A method using gray level aura (GLAM) matrix as a feature extractor and K-nearest neighbor (KNN) as a classifier was developed by Hanna et al. [14]. The method provided a robust solution for automated solid waste bin level detection, collection and management. GLAM of an image measures the amount of each gray level occur in the presence of other grey levels in the neighborhood. Feature vectors were constructed by the aura measures of captured image frames. Samples of features were extracted from

training images and stored as references in the form of vectors. In the classification process, a feature vector is extracted from the captured frame and then compared to the stored reference vectors. K reference vectors that are nearest to the input feature vector are selected and the class of the input vector is determined by a majority vote of the classes of its nearest neighbors [15]. The system showed good classification rate but its accuracy dropped when the bin was shifted or rotated.

Islam et al, [16] came up with a solution for shifted bin using template matching and Dynamic Time Warping (DTW). DTW is a pattern matching algorithm which finds the warping path of two patterns from their distance metric [17]. First, the captured image was scanned section by section to find the location of the bin using a template of the bin as a reference. The similarity between the section of the image and the template was measured using DTW. The section that registered the minimum score was considered as containing the bin. Then the features were extracted from the bin area using Gabor Filter (GF) and classified by Multi-Layer Perception (MLP) into several classes. However, the system requires a fixed camera position and bin orientation to operate effectively. Furthermore, the presence of square objects with size similar to the bin opening in the image affected its performance. The accuracy of the method fell the when the bin got rotated or overflown with rubbish and when square objects are present in the image.

W. A. Zaila et, al. [18] utilized Hough transform to extract line information from the entire image and used the line coordinates as a feature for bin level classification. In their work, gradient information is used with Hough transform to find lines in each frame. Then using the voting procedure of Hough Transform the coordinates of edge lines with high intensity are extracted and used to detect the presence of waste inside and outside of the bin. They claim that a good classification is achieved in detecting the presence of waste outside the bin. However, the accuracy of the waste level in the bin is

only 82.93%. This is because the edge information is obtained from the entire image rather than just from inside the bin area. Furthermore, there is no guarantee that the rubbish will always display strong linear edge gradient especially when their shape is arbitrarily nonlinear. Since no attempt is made to locate the bin opening, it is assumed that the level of rubbish in the bin corresponds to the number of lines detected in the whole image, which is not always accurate.

2.12 Summary

In this chapter a literature survey on brief algorithm and applications of HMM and SVM are presented. These sections are followed by the descriptions of image processing algorithms which are relevant to the cases of the objectives. In the next sections EEG and EOG signals and their applications in wheel chair navigation systems are described. Finally a brief literature review on solid waste bin level detection is presented.

CHAPTER 3

Case Study 1: Eye Gaze Controlled Automated Wheel Chair Navigation System Using EEG

3.1 Introduction

In this chapter framework of wheel chair navigation system based on SVM and HMM is presented. In the following sections the methodology, feature extraction classification, experiment and the results of the case study is described in detail.

3.2 Methodology

Blinking and horizontal eye movement signals can be traced from dipolar artifacts in EEG signals [14]. The spectral amplitude of the trace in the alpha response is higher when the eyes are closed than when they are open [40]. Therefore, the eyelid position can be inferred from the trace obtained from the O2 occipital region. By contrast, the low frequency artifacts extracted from the delta rhythm of the frontal lobe are related to the horizontal eyeball movement. Hence, the user's gaze direction can be inferred from the frontal leads of F9 and F10 [95]. Another important cue extracted from the delta rhythm trace is blinking. Since both the natural and intentional blink exhibit the same cue, double blink is used instead.

In our experiments, the electrodes are placed at F9, F10 and O2 sites as shown in Figure 3.1. In the experiment, the earlobe is used as reference and FPz is taken as the ground.

The O2, F9 and F10 signals are sampled at 256 samples per second (Hz). The EOG trace in the O2 signal is obtained by bandpass filtering the signal with a Butterworth filter with a passband of 8-13Hz. The F9 and F10 signals are filtered with a Chebyshev

lowpass filter with a cutoff frequency of 4Hz. Then for each filtered signal, a window of 128 samples is analyzed every 0.5 second.

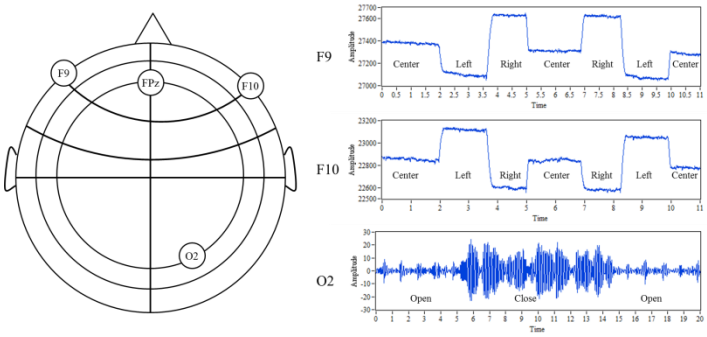

Figure 3.1: The positions of the electrodes and samples of their trace signals.

3.2.1 Open or closed eye classification

The alpha trace of channel O2 exhibits higher amplitude of signal fluctuation when the eyes are closed than when they are open as shown in Figure 3.2. The common amplitude of the signal is around 5-10uV when the eyes are open and 20 – 40μV when they are shut.

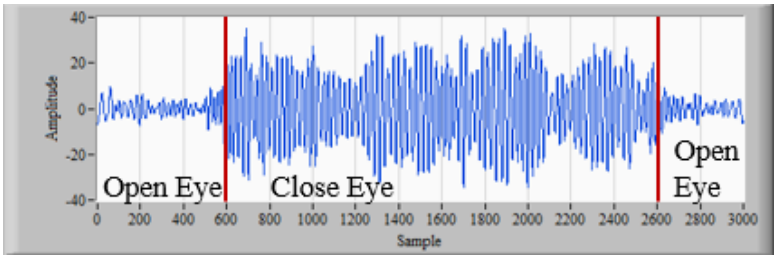

Figure 3.2: Alpha signal during closed and open eye.

From the alpha trace, two simple features can be calculated to distinguish closed from open eyes, variance and central tendency measurement (CTM). The variance (σ^2) of the 128 samples in the 0.5s window is given by

$$\sigma^2 = \frac{1}{N}\sum_{i=1}^{N}(x_i - \mu)^2 \tag{3.1}$$

where N is 128 and μ is the mean of the samples.

Central Tendency Measurement (CTM) is simply a 2D plot of sample difference. It is a plot of [*x(n + 2) – x(n + 1)*] against [*x(n + 1) – x(n)*] that displays the rate of variability in a time series. From this plot, the ratio of the samples that fall inside a circle of radius r over the total number of samples is calculated. Let N be the total number of points in a window frame. Excluding the end points there are N-2 points in the CTM plot. The CTM ratio is defined as

$$\delta(d_i) = \begin{cases} i & if \left([x(i+2) - x(i+1)]^2 + [x(i+1) - x(i)]^2 \right)^5 < r \\ 0 & otherwise \end{cases} \tag{3.2}$$

$$CTM = \frac{1}{n-2} \sum_{i=1}^{n-2} \delta(d_i) \tag{3.3}$$

We find that the CTM ratio of alpha trace is bigger during closed eye than open eye as shown in Figure 3.3. In our experiment, the radius of the circle (r) was fixed at 2. Both variance and CTM are used together to determine whether the eyes are closed or open.

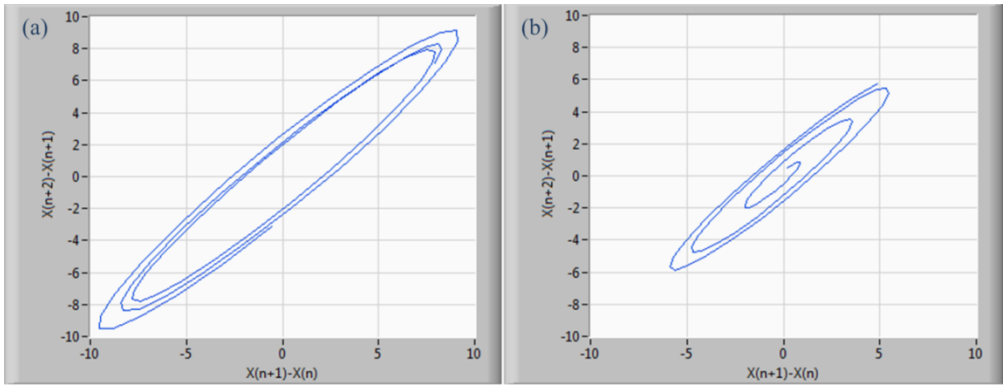

Figure 3.3: (a) CTM plot of closed eye alpha (b) CTM plot of open eye alpha.

3.2.2 Gaze direction classification

In our system, only three gaze directions are used and they are left, center and right. As the eyeballs move from one direction to another, voltage levels of the F9 and F10 traces changes in the opposite directions. For example, when the eye gaze shifts from center to left, the F9 trace decreases but the F10 trace increases by the same amount.

The same phenomenon is observed when the gaze moves from right to center. But when the eye gaze moves from center to right or from left to center, the F9 trace increases while the F10 trace decreases.

The eye gaze can also shift directly from left to right or the reverse. When this happens, a higher jump in voltage levels in F9 and F10 traces is observed as shown in Figure 3.4. This is probably due to a full distance shift by the eyeballs going from corner to corner as compared to a half distance shift from center to corner (or corner to center). To accentuate the effect of the opposite voltage level movements in F9 and F10 traces caused by gaze shift, we subtract F10 from F9 and extract two features from the difference signal. They are the voltage level rise and average first derivative. The derivative of the i^{th} sample is defined as

$$d_i = \begin{cases} |x_{i+a} - x_i| & if\ i < a \\ |(x_{i-a} + x_{i+a})/2| & if\ a < i < n-a \\ x_i - x_{i-a} & if\ i > n-a \end{cases} \tag{3.4}$$

Where, n = 128 and a = 5 in our experiment. Then the average of the first derivatives (f) is calculated as

$$f = \frac{1}{n}\sum_{i=1}^{n} d_i \tag{3.5}$$

The two features are fed to a series of SVM classifiers that classifies a gaze shift into 5 classes which are unchanged, half right, half left, full right and full left. Full right is the corner to corner gaze shift from left to right, while full left is the corner to corner gaze shift from right to left. Half right and half left are semi gaze shift to the right and left respectively. Half right represents either a center to right or left to center gaze shift since they both produce the same voltage level change. Similarly, half left represents either a center to left or right to center gaze shift. Knowing the eye gaze direction prior

to half left or half right gaze shift, allows the system to determine the final gaze direction.

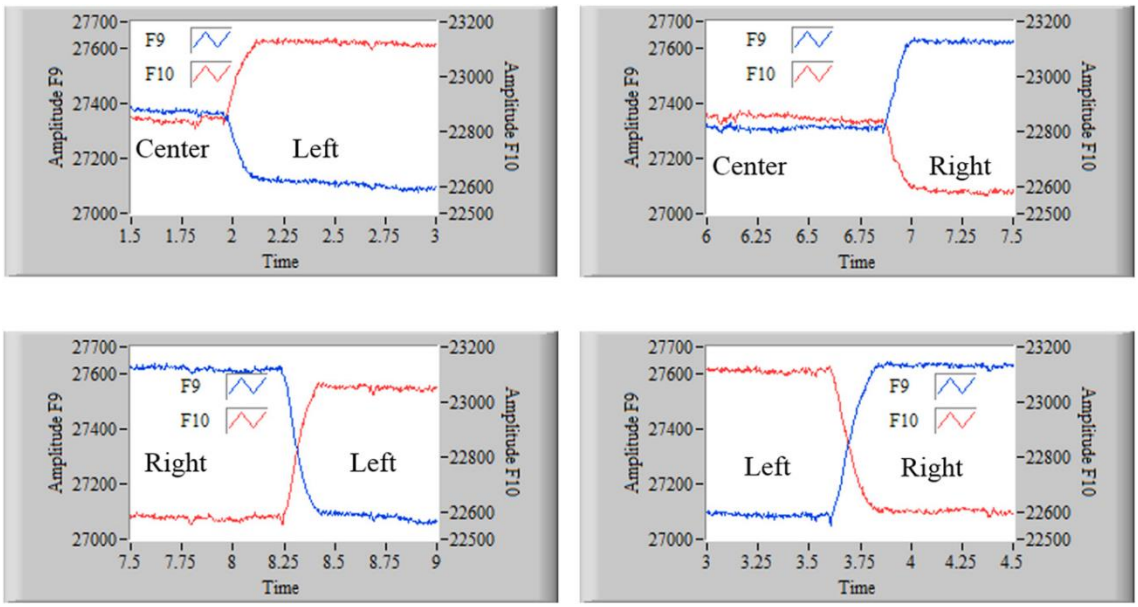

Figure 3.4: Samples of voltage jumps caused by gaze shifts

3.2.3 Double blink detection classification

When the user blinks his eyes, intentionally or otherwise, a short positive pulse or spike is detectable in both the F9 and F10 signals temporarily. Therefore adding F9 and F10 signals should accentuate the blink signal and attenuate the effect of horizontal eye movement as shown in Figure 3.5. Since natural and intentional blinks generate identical pulse in the added signal, they are indistinguishable. Thus, a double blink is used instead as one of the instructions in the system. Since a double blink consists of two close blinks, two spikes or pulses should be observed within two consecutive window frames. Variance and average first derivative can be extracted from the sum signal (F9 + F10) to detect the presence of a double blink.

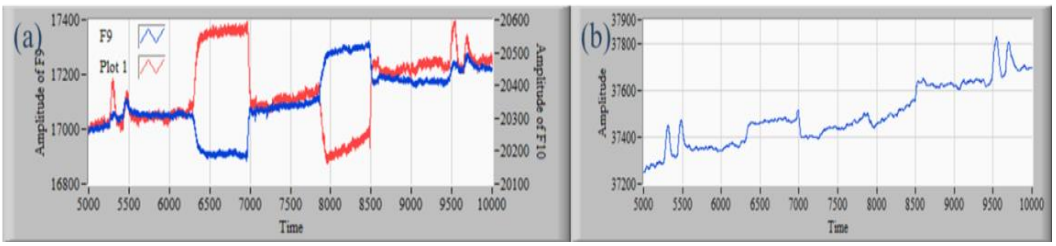

Figure 3.5: (a) EEG signal pattern of F9 and F10 Channels when blinks. (b) Added pattern of EEG signal.

3.2.4 Sliding window

While monitoring the alpha trace, a conventional window frame might capture an interval when the eyes are just about to open or shut. During this short period, the signal is in transition from low amplitude to high or vice versa. In this case, the samples in the window are a mixture of those with low and high amplitudes as shown in Figure 3.6. Consequently, the variance obtained neither represents open nor closed eye condition. Therefore, a sliding window is used to adjust the position of the frame so that it will either contain samples of closed or open eye exclusively.

First, the absolute values of the samples in the window are divided into 8 adjoining subintervals where each subinterval contains 16 samples. Then the average of samples in each subinterval is calculated and the averages of the first and last subinterval are compared. If the absolute difference of the two averages is more than a specified threshold, the window is shifted to the right by 16 samples. The process is repeated until their difference is less than the specified threshold. Once this condition is met, the variance and CTM of the samples in the whole window can be calculated.

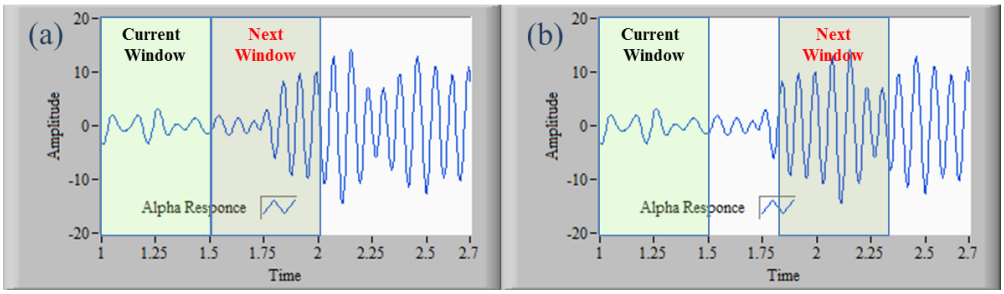

Figure 3.6: (a) Conventional window, (b) sliding window capturing close eye in alpha rhythm.

For the sum and difference signals of the F9 and F10 traces, the position of the window is also adjusted so that an important cue will be at the center of the window as illustrated in Figure 3.7. This step is necessary to obtain high classification accuracy. First, the samples in the window are divided into 8 adjoining subintervals where each subinterval contains 16 samples. Then the average first derivative of samples in each subinterval is calculated and the averages from the first and last subinterval are compared. If their absolute difference is more than a specified threshold, the window is shifted to the right by 16 samples. The process is repeated until the difference is less than the threshold. Once this condition is met, the variance, VLD and AFD of the samples are calculated.

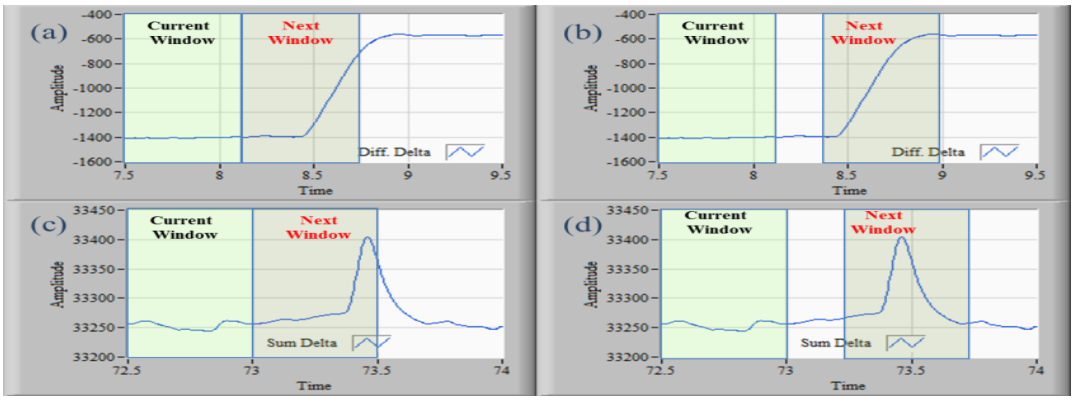

Figure 3.7: (a) Conventional window capturing part of a cue in difference signal, (b) sliding window capturing the full cue, (c) conventional window capturing part of a cue in sum signal and (d) sliding window capturing the full cue.

3.2.5 SVM Classifier

An SVM is a binary classifier that is useful for segregating the input features into two classes. For closed or open eye classification using the alpha trace features only a single SVM is sufficient. This is also true for the double blink detection using features from the sum signal. However, to classify the gaze shifts using features from the difference signal, four SVMs are needed. The first SVM determines whether the gaze is shifted or not. If the gaze is shifted, the second SVM decides whether the shift is to the left or right. If the gaze is shifted to the right, the third SVM will further classify it into full or half shift. Similarly, if the gaze is shifted to the left, the fourth SVM will determine whether the left shift is half or full. The classification process is depicted in Figure 3.8. Using the outcome of this classification and the initial gaze direction (prior state), the HMM will decide the current gaze direction (current state) of the system and the appropriate command for the wheelchair.

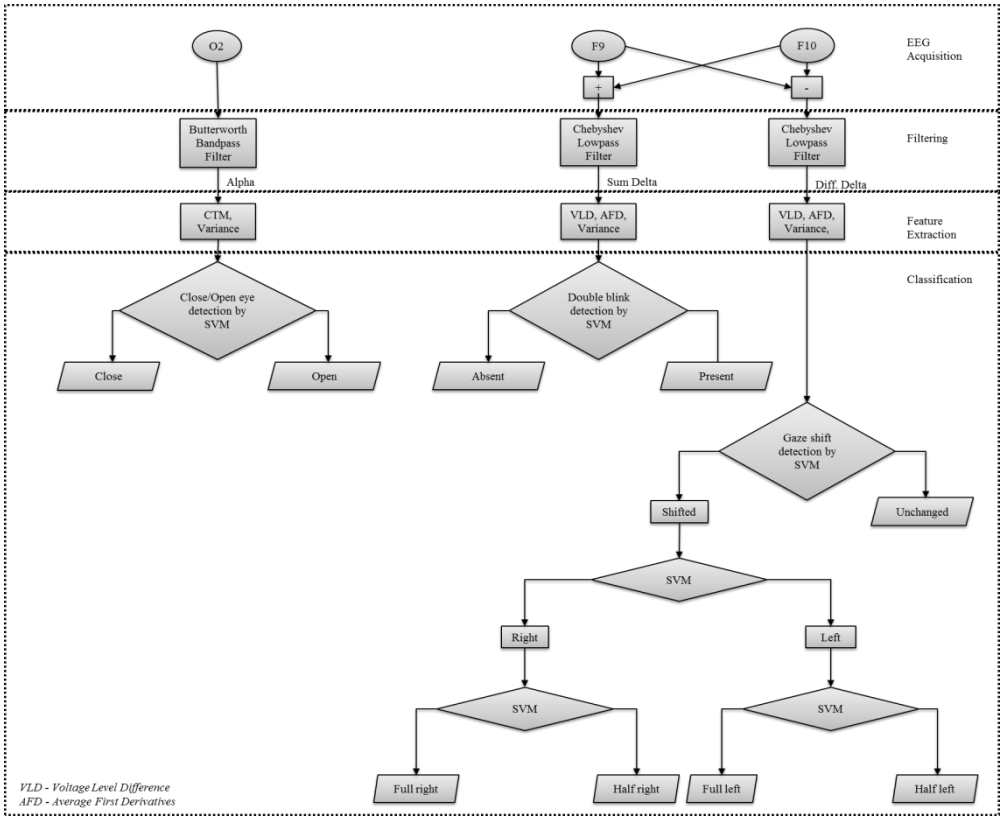

Figure 3.8: Flow of classification process

3.2.6 Hidden Markov Model (HMM)

The system is designed to allow the wheelchair to move forward and backward in three different directions. It should be able to stop as well. However, there are only a limited number of distinct horizontal eyeball movements and they are insufficient to move the wheelchair in 6 different directions. Another problem is that, left to center and center to right gaze shifts produce the same voltage change in the difference trace signal. This is also true for right to center and center to left gaze shifts. Thus, we resort to using an HMM to tackle this challenge.

An HMM is a statistical model where the state is not directly visible. In our case, the state is left, middle or right. The transition from one state to another is governed by the features extracted from the alpha and delta traces. The probability of the current state of the model $P(S_t|Model)$, is obtained by multiplying the transition probability of the previous state to current state $P(S_t|S_{t-1})$ and the probability of detecting the current observation given the current state $P(O_t|S_t)$. The gaze direction that maximizes the product of the probabilities is chosen as the current state as stated in the following equations.

$$P(S_t \mid Model) = P(S_t \mid S_{t-1}).P(O_t \mid S_t) \tag{3.6}$$

$$S_t = \arg\max(P(S_t \mid Model)) \tag{3.7}$$

It is assumed that the previous state is known. At the beginning (t = 0), when the previous state does not exist yet, the initial probability $P(\pi)$ is used to replace the transition probability $P(S_t|S_{t-1})$. Details on the fundamental and implementation of HMM are available in [54]. The hidden markov model is shown in Figure 3.9.

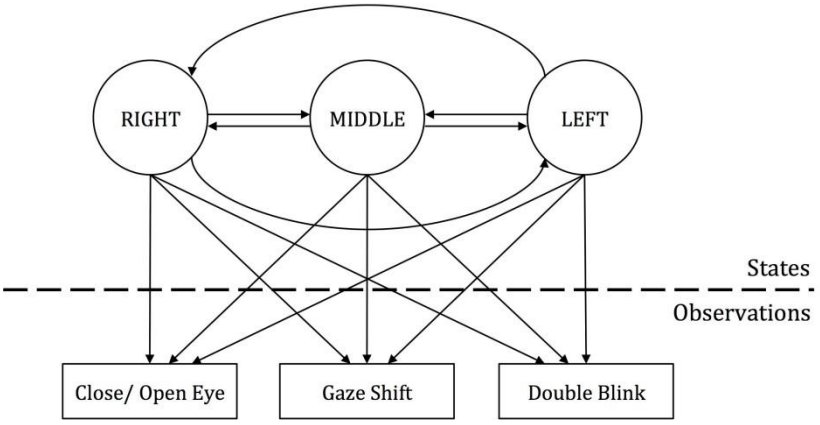

Figure 3.9: Hidden Markov model.

3.2.7 The overall system

The system is designed to have two modes of operation namely the ready and run mode. Both modes contain three states which are right, middle and left. In both modes, the state of the system follows the gaze direction of the eyes. The O2, F9 and F10 traces are analyzed every 0.5 second. Features extracted from these signals are used to inspect the condition of the eyes whether they are closed or open, the occurrence of double blink and gaze shift.

The ready mode allows the system to be executed at software level only so that the user can train and check the system functionality while the wheelchair is stationary. This mode also allows the user to select either forward or backward as the direction the wheelchair will go when it enters run mode. For run mode, both the software and hardware of the system are fully functional. In this mode the wheelchair will move according the gaze direction. It can move straight, turn left or turn right, in forward or backward direction. It stops if the user closes his eyes or double blink.

When the system is turned on, it is assigned to the middle state of the ready mode by default. The state should follow the gaze direction of the eyes at all time. If the state of the system fails to follow the gaze shift correctly, an error occurs. The system is designed to correct minor errors automatically but inform the user when a major error is

detected. A minor error occurs when the state is correct but the command signal is wrong. For instance, the current state is middle but the command asks the system to move the state from left to right. In this case, the system will just move the state from center to right. A major error occurs when the state is wrong and a command cannot be executed at all. For example, the state is right and the command is to move the state from left to right. In this case, the system cannot execute the command as the state is already right. Thus, the system will alert the user to move his gaze to the center and reset its state to the middle. For whatever reason, the user can also reset the system manually by closing her eyes for at least 3 seconds.

Once the user is familiar with the system, she may want to command the wheelchair to move. The first step is to choose the direction the wheelchair will go when entering the run mode, either forward or backward. The move direction is chosen by shifting the state to the right or left, for forward or backward direction respectively. Then the user should maintain her gaze in that direction for at least 3 seconds or 6 consecutive frames to lock the chosen direction. The user can change the move direction by gazing at the opposite direction and maintaining her gaze for at least 3 seconds. But if the user wants to unlock the move direction, she simply has to shut her eyes for at least 3 seconds. This action unlocks the move direction and returns the system to middle state of ready mode. The user is expected to set her gaze to the center when opening her eyes so that her gaze will match with the default state. Once a move direction is selected and the user is ready to move the wheelchair, he should blink twice to send the system into run mode immediately. This is a backup measure to correct a major error if the system fails to correct it automatically.

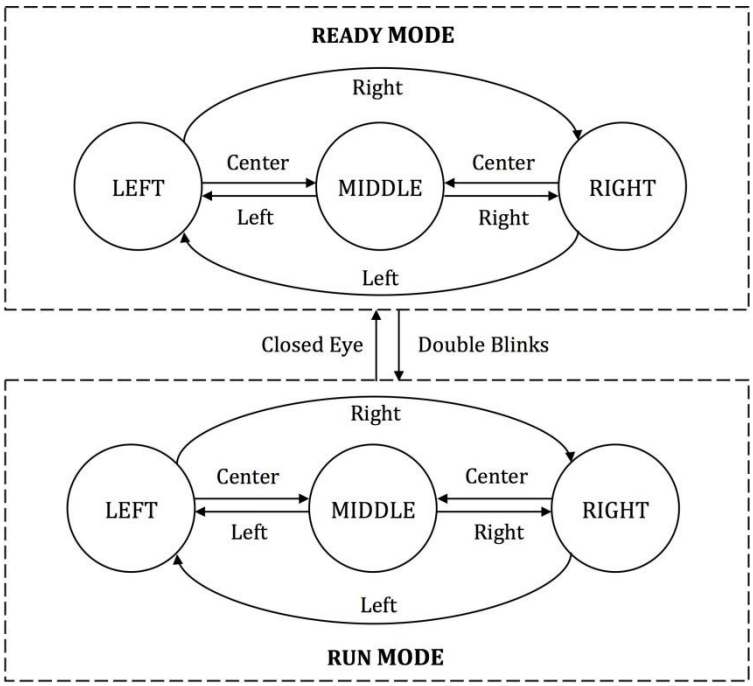

Figure 3.10: The modes and states of the system.

Upon entering the run mode, the user is given 3 seconds to direct his gaze to where he wants to go before it is taken as the first instruction to move the wheelchair. Each instruction will be executed for at least 2 seconds to maintain the stability of the moving wheelchair and avoid command overcrowding. Another restriction is that the wheelchair will stop before turning or changing direction. And finally, only a gradual change of direction is allowed. An abrupt change of direction from left to right or vice versa will be executed with an intermediate step of going straight for 2 seconds. For instance, if a user wishes to change the direction of the wheelchair from right to left, the wheelchair will change direction gradually from left to straight first before turning left. This is to prevent the wheelchair from toppling over. At all time, the wheelchair is moving at 5km/h. If a user wishes to stop the wheelchair, all she has to do is close her eyes for at least 0.5 second so that the system will terminate whatever command it is executing and stop. This action makes the system exit run mode and sends it to middle state of ready mode without unlocking its move direction. If the user wishes to re-enter

the run mode, he has to double blink as before. In ready mode, the user can also select a new move direction, reset the system or rest.

It should be noted that in run mode, double blink cue is not used. This is because detecting a double blink is more time consuming as it occupies two consecutive windows. The last point to note is that in a span of two seconds, only one command is kept for the next move while the wheelchair is executing the current instruction. If the user produces multiple instructions within that interval, only the latest is kept as the next command to be executed.

3.3 Experiments

The EEG signals are recorded using g-USBAMP toolkit from Guger Technology at a sampling rate of 256Hz. Silver electrodes are placed at five different locations on the scalp according to the standard International 10–20 system. The locations are F9, F10, O2 with earlobe as reference and FPz as ground. These locations are selected since they contain the strongest EOG trace in filtered signal with minimum noise. The horizontal gaze movement and blink are interpreted from the F9 and F10 channels. Close and opened eye condition is inferred from the O2 channel. The recorded signals are analyzed using LabView software of National Instrument. The window size is 0.5s since it is the smallest possible for capturing a blink pulse.

The experiments are conducted in three sessions namely the offline, online and navigation session. In the offline session, the user is exposed to the system functionality and data are collected to train the SVMs and HMM, and determine the values of thresholds needed for sliding window adjustment. This is followed by an online session where the user is asked to move the wheelchair according to randomly chosen instructions. Lastly, a real time navigation session wherein the user is asked to navigate

the wheelchair along two routes is performed. Details of the experiments in each session are described in the following section.

3.3.1 Offline session

The objectives of the training session are to check the system condition and record alpha and delta signals for calculating thresholds and training the SVMs and HMM. This session is conducted in ready mode and thus the wheelchair is stationary. A series of instructions are issued to the user and the time allocated for each instruction is 5 second. Then a 5 second break is given before the next instruction is issued. Turn left, turn right, go straight, double blink and close eye are the five possible instructions that are randomly assigned. The participant is expected to respond within 2 seconds after the instruction is announced. The change in states and modes are shown by the LED display on the user interface. If any of the instruction is wrongly or not executed, the instruction is repeated. Altogether, 100 instructions must be executed by each participant and the output signals recorded.

3.3.2 Online Session

The online session is conducted in run mode and thus the wheelchair will move according to the user's commands. First, each participant is instructed to lock the move direction to forward and enter the run mode. In run mode, there are only 4 possible instructions which are turn left, turn right, go straight and close eye. In total, 20 instructions are assigned to each participant, 5 from each command. The instructions are randomly assigned every 5 seconds without break. Upon hearing a command, the participant is expected to perform it accordingly. A command is considered successfully executed if the user is able to move the wheelchair correctly in less than 2 seconds.

Next, the participant is instructed to change the move direction to backward. Then 20 instructions are assigned to each participant randomly, 5 from each command as

before. Throughout this session, changes in the state are also displayed on the user interface panel by LED lights. After that the participant is given 30 minutes to tinker with the system freely to gain more familiarity before the navigation session commenced.

3.3.3 Navigation Session

Two routes are designed to allow the user to navigate in indoor environment as shown in Figure 3.11. The passage width is in the range of 4.5m to 1.5m. The first route is shorter and its total optimal length is 13.5m with four checkpoints of A_1, B_1, C_1 and D_1. The second route has a total optimal length of 54.4m with seven checkpoints from A_2 to G_2. The participants are responsible for maneuvering the wheelchair to pass through these check points starting from the first point to the last point and then return to the first point. However, when the participants reach the dead end points of D_1 (in Fig. 11 (a)) and G_2 (in Fig. 11(b)) they are expected to reverse the wheelchair backward to exit the tight end and only make a u-turn at point C_1 and F_2 respectively. Each participant is given 3 attempts to repeat the task and at the end of the session they are asked to answer a set of questionnaires regarding their experience.

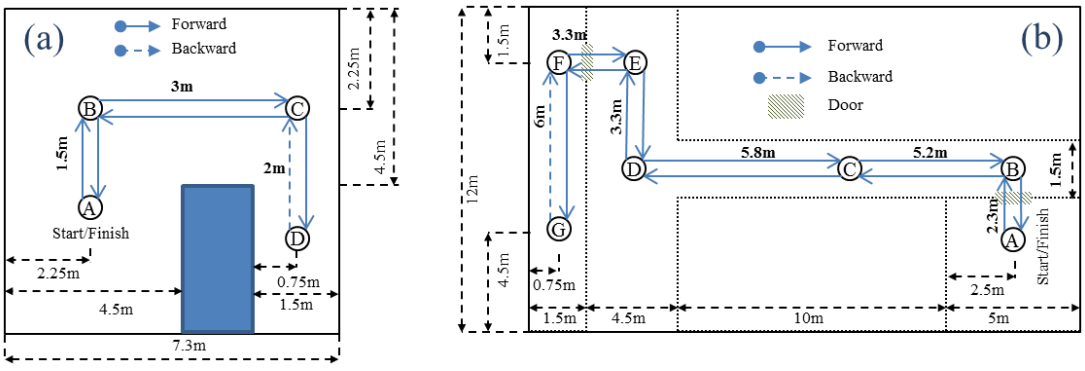

Figure 3.11: The navigation route with checkpoints (a) Route 1 (b) Route 2.

3.3.4 Hardware implementation

From the result of the classifier, a command to the wheelchair is identified and issued. The system checks whether it is the same command that is currently being executed. If it is the same, the execution of the current command is prolonged. If it is different, a new instruction in the form of a digital command is sent to a digital to analog module that converts the digital signal to an analog voltage level. The module used in our experiment is NI9264 by National Instrument. The analog output is then sent to a motor controller that controls the right and left motors of the wheelchair as shown in Figure 3.12 (a). The controller will switch on the right, left or both motors if the command is turn left, turn right or move forward respectively. If shut eye is detected, both motors will stop and the system will exit run mode and enter ready mode at middle state. The mode, move direction and current state are all displayed in front of the user by led lights as shown in Figure 3.12 (c).

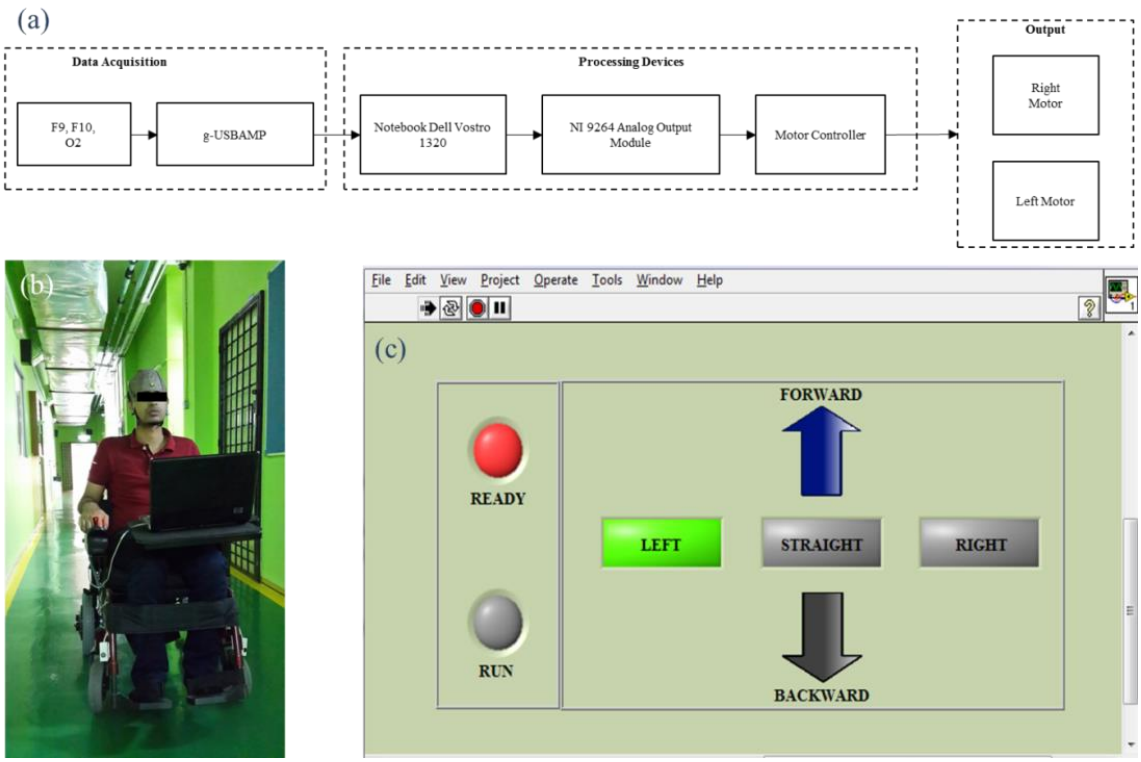

Figure 3.12: (a) Diagram of integrated system (b) a subject undergoing the experiment (c) print screen of the user interface.

3.4 Results and Discussion

3.4.1 Offline and online session results

A total of 20 healthy subjects participated in the offline and online sessions. They are mainly undergraduate and postgraduate students with no neurological impairments or nystagmus. Other data on the subjects are given in Table 3.1. In the offline session, the participants were required to perform double blink, eye close and horizontal saccades to the left and right. Altogether, 2000 signals were recorded from the participants. Features extracted from the EOG traces were used to train the SVMs and calculate the thresholds necessary for the sliding window operation.

Table 3.1: Average height, weight, gender and corrective lenses of the subjects according to age groups

Age Group	Avg height (cm)	Avg weight (kg)	Male	Female	Wearing lenses
20-23	167.33	62.33	2	3	2
24-27	169.02	73.14	8	2	4
28-31	171.33	65.52	2	1	0
32-35	152.50	61.20	0	2	2

This is followed by the online session where participants were instructed to execute the four commands in forward and backward directions. Throughout the session, each of the four commands was performed 100 times in the forward and then backward direction. The summary of the online tests is presented in the confusion matrix of Table 3.2. Overall, the total execution rate is 98%. It can be observed that the go straight and close eye commands are perfectly classified and executed. Six turn right and eight turn left commands are wrongly executed. Out of these errors, 8 commands are not executed within 2 seconds and the remaining six errors are corner to corner gaze shifts that are wrongly interpreted as corner to center shift. This is mainly due to the user failing to shift his/her gaze from corner to corner rapidly. This generates weaker pulses in F9 and F10 that are similar to the ones generated by corner to center gaze shift. Factors that may cause this error are fatigue, inattention and distraction. Another possible cause is

the wheelchair movement that might lead to head or body movement, which could result in unwanted EEG or EOG artifacts. The artifacts might in turn affect the accuracy of command estimation.

Table 3.2: Confusion matrix for system errors in direction estimation.

Command	Actions	Right-Middle	Left-Middle	Middle-Right	Left-Right	Middle-Left	Right-Left	Close Eye	Not Executed
Go Straight	Right-Middle	100	0	0	0	0	0	0	0
	Left-Middle	0	100	0	0	0	0	0	0
Turn Right	Middle-Right	0	0	98	0	0	0	0	2
	Left-Right	0	3	0	96	0	0	0	1
Turn Left	Middle-Left	0	0	0	0	97	0	0	3
	Right-Left	3	0	0	0	0	95	0	2
Stop	Close Eye	0	0	0	0	0	0	100	0

A comparison with similar wheelchair navigation studies is given in Table 3.3. Although the classification rate achieved by Rebsamen et al. [8] is slightly higher, the execution time of their system is way higher than 1 second. On top of that, our system features backward movement, which is not available in other systems. Furthermore, they employed P300 synchronous system, which requires the user to follow the system pace.

3.4.2 Navigation session results

Five participants with the highest score in the online session were selected to perform the navigation tests. Then the performances of the wheelchair system and the participant were evaluated according to the following criteria.

1) Task Success: Completion of the navigation through the end of path.

2) Path length: Distance in meter traveled to accomplish the task.

3) Time: Time in seconds taken to accomplish the task.

4) Path Optimality Ratio: Ratio of the path length to the optimal path (the optimal path was 13.5m for Route 1 and 54.4m for Route 2. See Figure 5)

5) Time Optimality Ratio: Ratio of the time taken to the optimal time to complete the task (the optimal time was approximately 9.7s for Route 1 and 39s for Route 2 based on maximum and rotational velocities of 1.39m/s and 0.4rad/s)

6) Collisions: Total number of collisions during the tasks. A collision is not considered a failure as long as the system is able to continue with a new command, or requires a brief intervention from the supervisor.

7) Mean velocity: Mean velocity in meter per seconds during motion.

8) Useful Accuracy: Ratio of correct selections to the total number of selections.

All subjects succeeded in navigating the wheelchair along the routes without collision. The results of the corresponding metrics are summarized in Table 3.4. The average distances travelled by the participants were 15.76 meter and 75.42 meter for route 1 and route 2 respectively. The path optimality ratios were low (1.17 for route 1 and 1.35 for route 2) which suggests that the participants were able to travel close to the designated paths. The average times to traverse the routes were 15.04 and 85.67 second for route 1 and route 2 respectively. On average the ratio of the optimal times were 1.55 for route 1 and 2.05 for route 2. The participants took longer time to complete the second route as it has more turns and longer narrow passages. The actual time is higher than the optimal time as it includes mode changing, command selection and computational time. The mean velocity of the wheelchair was 1 m/s for first route. For the second route the participants had lower a velocity 0.88 m/s. The maximum speed was limited to 1.3 m/sec for safety reasons. The useful accuracy is 98% for route 1 and 97% for route 2. In general, a narrow performance gap observed among the participants

signifies the system usability and consistency to navigate and maneuver the wheelchair in open and small space.

Table 3.3: Comparison between this study and other HMI system used for wheelchair navigation.

	HMI system		Classifier	Classification accuracy (%)	Time(s)
Huang et al. (2012) [31]	Imagery	Synchronous	Mahalanobis Linear Distance (MLD)	84.3	60.4
Kus et al. (2012) [32]	Imagery	Asynchronous	MLD	74.84	8.81
Choi et al. (2013) [33]	Imagery + SSVEP + P300	Asynchronous	SVM, CCA and Bayesian	84.4 – 91	27.2
Long et al. (2012) [34]	Imagery + P300	Asynchronous	LDA	83.10	6
Rebsamen et al. (2010) [12]	P300	Synchronous	SVM	99.78	6
Iturrate et al. (2009) [35]	P300	Synchronous	Stepwise Linear Discriminant Analysis	94	5.40
Diez et al. (2011) [36]	SSVEP	Asynchronous	Fourier transform	81.68	4.48
Parini et al. (2009) [37]	SSVEP	Asynchronous	LDA	97.5	2.38
Postelnicu (2012) [55]	EOG	Asynchronous	Fuzzy Logic	95.63	2.6
Proposed study	EEG + EOG	Asynchronous	SVM and HMM	98	0.68

Table 3.4: Metrics to evaluate the Navigation Performance.

	Task 1				Task 2			
Factors	min	max	mean	std	min	max	mean	Std
Task Success	1	1	1	0	1	1	1	0
Path Length	13.87	17.14	15.76	1.17	55.46	95.57	75.42	19.27
Time	12.66	17.86	15.04	1.93	67.52	117.06	85.67	18.84
Path Optimally Ratio	1.03	1.27	1.17	0.09	1.02	1.76	1.35	0.32
Time Optimally Ratio	1.30	1.84	1.55	0.20	1.52	2.99	2.05	0.51
Collisions	0	0	0	0	0	0	0	0
Mean Velocity	0.90	1.12	1.00	0.10	0.64	1.09	0.88	0.18
Useful Accuracy	0.95	1	0.98	0.01	0.95	1	0.97	0.02

3.4.3 Participant Experience Evaluation

At the end of the navigational session, the participants were given a set of questionnaires to express their navigational experience in three metrics of average workload, learnability and confidence as presented in Figure 3.13. The metrics were measured in scale between 0 and 5 from the least to the most. The workload metrics

denotes the effort to accomplish the tasks. All participants agreed that it took a higher workload to complete Route 2 than Route 1. Because of the route 2 has more turns and narrower passage than the route 1. Participant P3 and P5 recorded the most effort required to operate the wheelchair in both route. The learnability metrics indicates that the participants adapted to control the navigation system based on their experience from the previous attempt thus increasing their confidence to perform the task.

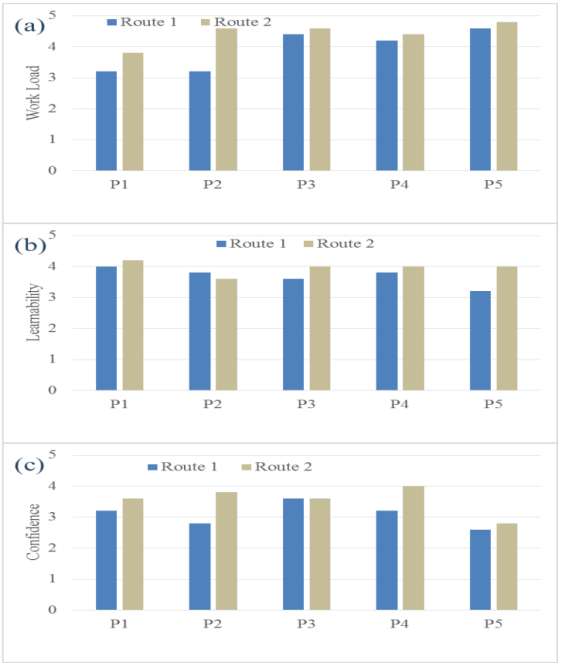

Figure 3.13: The assessment of the participants' navigational experience as (a) work load (b) learnability (c) confidence. The scale of 0–5 (least to the most) was used to express the metrics.

At the end of the navigational session, the participants were given a set of questionnaires to express their navigational experience in three metrics of average workload, learnability and confidence as presented. Figure 14 shows the workload, learnability and confidence metrics of the navigation experiment. The metrics were measured in scale between 0 and 5 from the least to the most. The workload metrics denotes the effort to accomplish the tasks. The participants reported significant increase in work load for route 2 than route 1 (Mean = 3.92 vs 4.44, $t(4) = -2.23$, $p = 0.04$). This

is because route 2 has more turns and narrower passage than route 1. Participants also reported increment in learnability from route 1 to route 2 (Mean = 3.68 vs. 3.96, $t(4) = -1.72$, $p = 0.08$). The learnability metrics indicates that the participants adapted to control the navigation system based on their experience from previous attempts. Their confidence was same to perform the tasks (Mean = 3.56 vs. 3.08, $t(4) = 2.59$, $p < 0.05$). Figure 3.14 shows the workload, learnability and confidence metrics of the navigation experiment.

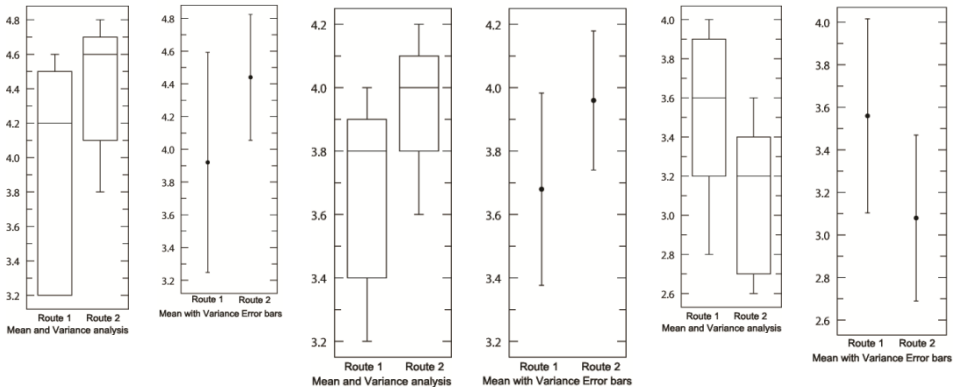

Workload Learnability Confidence

Figure 3.14: Workload, learnability and confidence metrics of the navigation experiment

3.5 Summery

In this chapter, the methodology of the first case study about wheel chair navigation system controlled by EOG traces in EEG is described. The methodology includes signal acquisition, feature extraction, classification, state estimation and wheel chair navigation processes. The wheel chair can be steered in total six directions as three direction forwardly and three direction backwardly. The results of every step are compiled in the result and discussion section of the chapter. The asynchronous system achieved an average classification rate of 98% in an online test with an average execution time of less than 1s.

CHAPTER 4

Case Study 2: Solid Waste Bin Level Classification and Collection Scheduling

4.1 Introduction

In this chapter the system of solid waste bin level classification and garbage collection scheduling using SVM and HMM is presented. In the following sections the methodology and the result of the system is described in detailed.

4.2 Methodology

An automatic waste level detection system should be robust against bin shift, rotation, occlusion of the bin opening by large objects and confusion from objects littered outside the bin. To achieve this objective we propose a system that detects the bin opening area and extracts features from it. Then the features are used as inputs to a classifier that determines the waste level in the bin. The system is used to detect 3 bins in captured image and schedule their collection sate using HMM. Figure 4.1 shows the flowchart of steps in the proposed algorithm. Details of each step of the algorithm are given in the following subsections.

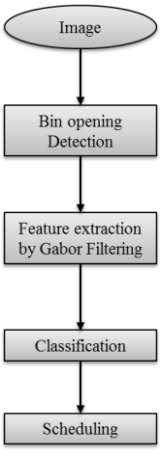

Figure 4.1: Flow of steps involved in the proposed method.

4.2.1 Image

The images are 800x600 pixels in size and they are captured with a low cost camera positioned above the bin. The bin is rectangular in shape and its area is approximately 300x300. Samples of some bin images with different waste levels are shown in Figure 4.2.

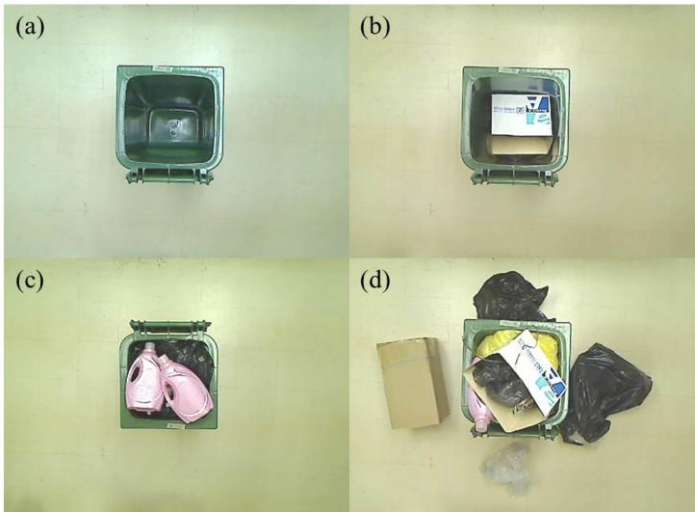

Figure 4.2: Samples of bin images at different waste levels (a) empty, (b) partial (c) full and (d) overflowing.

Figure 4.3: Bin database samples at different levels (a) empty-empty-empty, (b) empty-empty-low, (c) empty-low-full, (d) full-full-full, (e) overflow-overflow-full and (f) toppled-low-full.

4.2.2 Bin Opening Detection

Assuming that the bin is upright, the bin opening is the area that contains the waste. To detect this area, we must first locate the four corners and the edge of the bin opening. So the first step is to obtain the edge information of the image using Canny Edge Operator before employing Hough Transform to detect straight lines in the edge image [53]. The Hough transform only provides two parameters for each line detected in the image. They are the magnitude of the vector from the reference point to the nearest point on the line and the angle formed by the vector and the horizontal axis at the reference point. In the line equation these parameters are normally represented by ρ and θ, and the line equation can be written as;

$$ax + by = \rho \tag{4.1}$$

Where, $a = cos\ \theta$ and $b = sin\ \theta$. A table consisting of all possible combinations of ρ and θ is rendered and for each pair of ρ and θ, the total number of edge pixels that fall on the line that the two parameters represent is recorded. Thirty lines with the most number of edge pixels are analyzed and the length of each line is checked to see whether it belongs to the bin contour. But more importantly, the intersection points of two orthogonal lines are sought because they are candidates for bin corners. When two lines are intersecting at point (x, y), equation (4.1) can be written for both lines at (x, y) as follows:

$$a_1 x + b_1 y = \rho_1 \tag{4.2}$$

$$a_2 x + b_2 y = \rho_2 \tag{4.3}$$

The orthogonality of the intersecting lines can be tested by multiplying a_1 by a_2 and b_1 by b_2 and summing their products. If the sum is zero or nearly zero then the two lines

are considered orthogonal. The point of intersection (x, y) for the orthogonally intersecting lines are obtained from;

$$x = \frac{\rho_1 b_2 - \rho_2 b_1}{a_1 b_2 - a_2 b_1} \tag{4.4}$$

$$y = \frac{\rho_1 a_2 - \rho_2 a_1}{a_2 b_1 - a_1 b_2} \tag{4.5}$$

If the bin is rotated, all of its corners will also be rotated by the same angle. For each corner candidate, the angle of rotation can be obtained from the θ parameter of one of the two lines that form the corner. Then a template of an empty bin is rotated according to the detected angle of rotation before it is superimposed on the corner candidate for similarity matching. The locations of the remaining three bin corners of the template are checked to see if they coincide with other corner candidates. If other candidates are present, the similarity matching is based on all of the candidates. Otherwise, it is calculated for a single candidate only.

The similarity between the corners in the image and the template is calculated using edge pixels along the intersecting lines only. In our work, correlation coefficient is chosen as the measure of similarity and it is calculated by the following equation.

$$Corr(I,T) = \frac{\sum_m \sum_n (I_{mn} - \mu_I)(T_{mn} - \mu_T)}{\sqrt{\left(\sum_m \sum_n (I_{mn} - \mu_I)^2\right)\left(\sum_m \sum_n (T_{mn} - \mu_T)^2\right)}} \tag{4.6}$$

Where, I is the candidate bin area in the image, T is the bin template, m and n is the pixel in I, and μ_I and μ_T are mean of pixel values of I and T respectively. The location of the template superimposed on the corner candidate with the highest correlation

values is considered as the correct bin areas. Bin areas as same number of bins supposed to be present in the image are considered for further processing.

4.2.3 Feature Extraction

Gabor filter is a Gaussian envelope modulated by a sinusoidal function. A 2-D Gabor filter can be written as [96];

$$G_{\sigma,\gamma,\lambda,\varphi,\theta}(x,y) = K \exp\left(-\frac{x'^2 + \gamma^2 y'^2}{2\sigma^2}\right)\cos\left(2\pi\frac{x'}{\lambda} + \varphi\right) \tag{4.7}$$

Where, $x' = x\cos\theta + y\sin\theta$, $y' = -x\sin\theta + y\cos\theta$, K is scale of magnitude, γ is spatial aspect ratio, λ wavelength of the sinusoidal function, φ is phase offset and θ rotation angle of the Gaussian envelope. Features used in the classification of the waste level are obtained by convolving the bin area in the image with a set of Gabor filters. At each pixel (x, y) in the bin area, the absolute value of the convolution of a Gabor filter and the pixels in the neighborhood centered at (x, y) is calculated. Then the absolute values of the convolution at all pixels in the bin area are summed to produce one feature. By changing the angle of rotation θ, a different Gabor filter is obtained and with this new filter another feature can be generated by repeating the same convolution process. Gabor filter features can also be obtained from the area outside of the bin in the image by following the same procedure.

4.2.4 Classification

The number of bin corners detected can be used as a feature for waste level classification. From the detected bin areas, a total of 4 more features can be extracted using four different Gabor filters. Then from the area outside of the bin, another 4 features are obtained using the same Gabor filters. So, altogether a total of 16 features

are used as inputs to four SVM classifiers to ensure the bin area and determine the waste level in the bin which can be empty, partially full, full or overflowing.

In our experiments, four SVM classifiers are used in the waste level classification. Radial Basis function is used as the Kernel. As a supervised classifier, an SVM requires training and 100 images of the bins with different waste level are used to train the SVMs before testing. Using the number of bin corners detected and the first four Gabor features first SVM is trained by accurate bin images as class 1 and incorrect bin candidates as class -1. As a result exact bin locations were figured out from the first level. If the number of area classified as exact bin location is less than the number of bins supposed to be found then it is concluded that the absent bins are topple over or removed from the expected location or fully occluded by the wastes. The second SVM decides whether the levels of exact bins are empty or filled. For the filled class, the third SVM takes the same set of input features and divides it into partially full and full classes. The last SVM operates independently of the first three. It takes the four Gabor features from outside of the bin area to check whether waste is littered outside the bin. However, the output of this classifier is only considered when the waste level of the bin is classified as full by the second classifier to identify overflowing cases. In deciding the four classes of the waste level, we assume that waste only starts to overflow after the bin is full. We do not consider the odd cases where rubbish is littered outside the bin when it is still empty or partially full. If these odd categories were to be included, they could be detected by considering the output of the fourth SVM for all cases. The classification steps are shown in Figure 4.4.

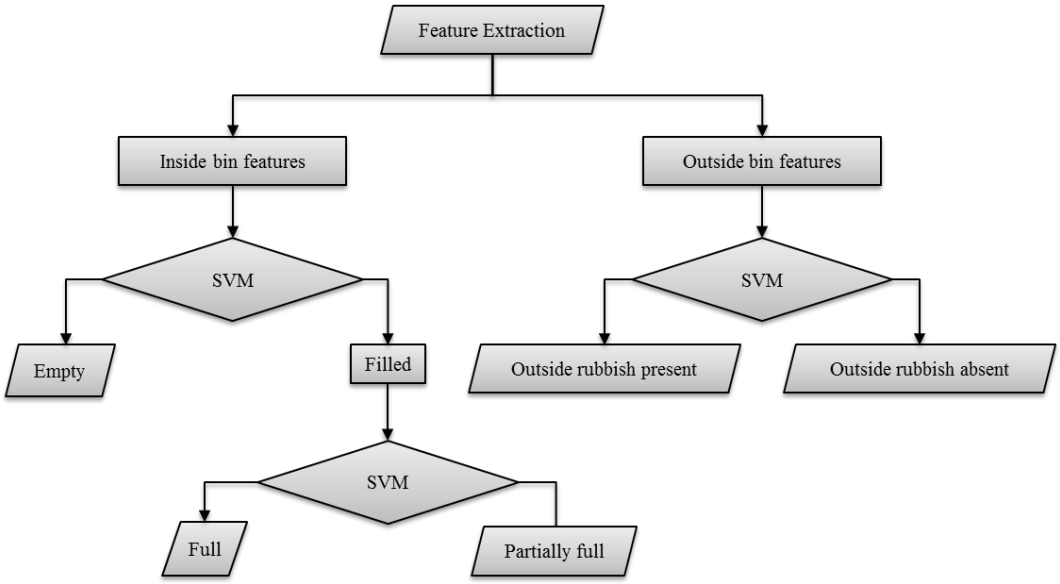

Figure 4.4: Bin level classification steps.

4.2.5 Scheduling

The collection schedule is related to the state of the HMM. The number of days left before the collection of garbage from the bins is related to the current state of the HMM which are not necessary, 3 day, 2 day, 1 day and immediate. The current state of the HMM is determined by rubbish levels in the bins and the previous state of the HMM. The observation and state transition are shown in

Table 4.1. The state starts from “Not Necessary” where all the 3 bin levels are empty. If bin levels are classified as low for any number of bins and all bins are detected then the state starts count down from three days. The state starts from 1 day if the levels found full for any number of bins and others are overflown but not absent. The state count down depends on the previous state where as the current state also depends on the observation. At the end of the count down the “Immediate” state indicates that the waste should be collected that instant. If any bin absent or three bins are over flown the state jumped to “Immediate” from any stage.

Table 4.1: State transition and observations of Bin collection scheduling

Bin	Observation	Previous State	Current State	Next State
Bin1	Empty			
Bin2	Empty	Any	Not Necessary	Not Necessary
Bin3	Empty			
Bin1	Low			
Bin2	Empty/Low/Full	Not Necessary	3 days	Count Down
Bin3	Empty/Low/Full			
Bin1	Full			
Bin2	Full/Over Flown	Not Necessary/More than 1 day	1 day	Immediate
Bin3	Full/Over Flown			
Bin1	Over Flown			
Bin2	Over Flown	Any	Immediate	Immediate
Bin3	Over Flown			
Bin1	Any			
Bin2	Any	Any	Immediate	Immediate
Bin3	Absent			

4.3 Experiments

The database consists of 300 images of single and 200 images of three 120L sized waste bin those are empty, partially full, full or overflowing with rubbish. Altogether there are %00 images of the bin at four different waste levels in the custom database. Each image is 800x600 pixels in size and the bin area is approximately 300x300 pixels. 100 images are used for training the SVM classifiers and the remaining 200 for single bin and 200 for three bin images are used for testing. For each image, greyscale conversion is performed to transform it into a grayscale image followed by edge detection using canny edge detector. The output is a binary edge image as shown in Figure 4.5.

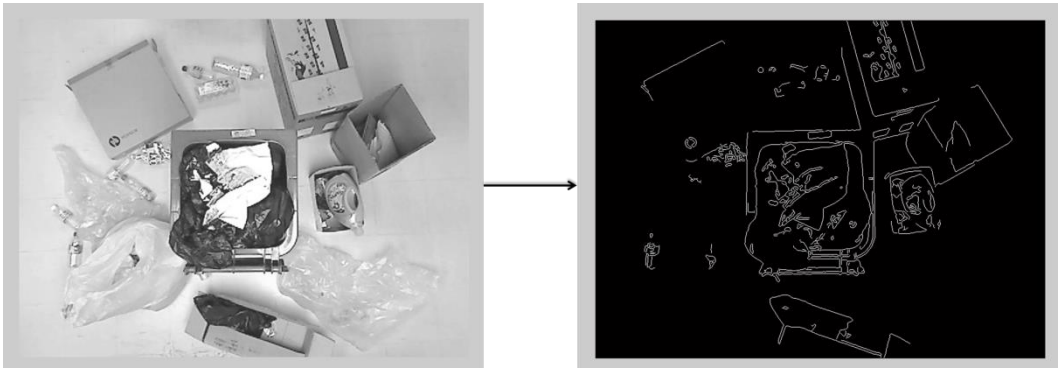

Figure 4.5: Edge detection of binary bin image.

Then line detection is performed on the binary image using Hough transform as shown in Figure 4.6. The aim is to detect the four sides of the bin opening and its corners. Each corner is represented by the intersection of two orthogonal lines. The position and orientation of the corner are obtained from the two intersecting lines that form the angle. Since rubbish with sharp corners and edge may be present in the image, a total of up to 20 corner candidates are considered in each image. Then each corner candidate is superimposed on one corner of an empty bin template after the template is rotated to match the orientation of the candidate. Correlation coefficient between the candidate and template corner is calculated using the edge pixels of the image and the template around the corner position.

In calculating the correlation coefficient of a candidate, if other candidates exist at the corners of the template area, they are considered collectively. Otherwise only the edge pixels of one corner are used in the calculation since the rest of the bin area is assumed covered by rubbish.

Once the bin area is determined, eight Gabor features can be extracted from the bin area and outside of the bin area using four different Gabor filters. The Gabor filters are obtained by fixing the values of θ at 0^0, 45^0, 90^0 and 135^0 as shown in Figure 4.7. The four Gabor features obtained from the bin area and the number of bin corners detected

is used as inputs to the first SVM to detect whether the bin is empty or filled. The second SVM uses the same five features to further divide filled category into partially full or full. And finally, the last SVM takes the four Gabor features extracted from the area outside of the bin to check whether waste is littered outside the bin.

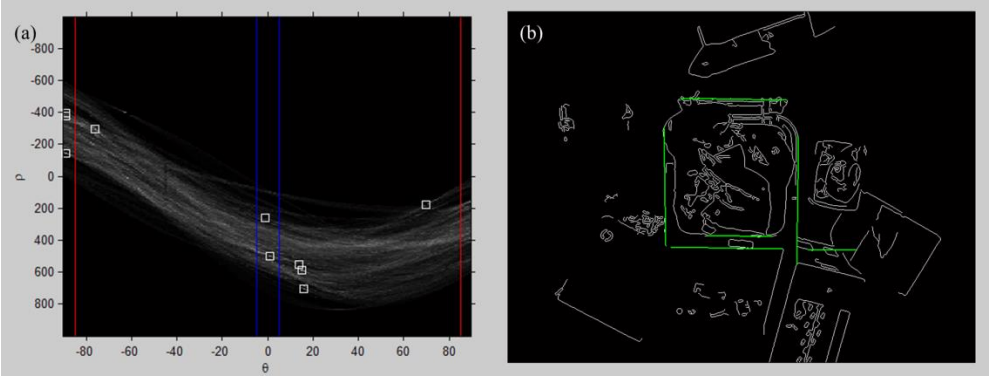

Figure 4.6: (a) ρ–θ plot of the lines detected in the image (b) detected lines.

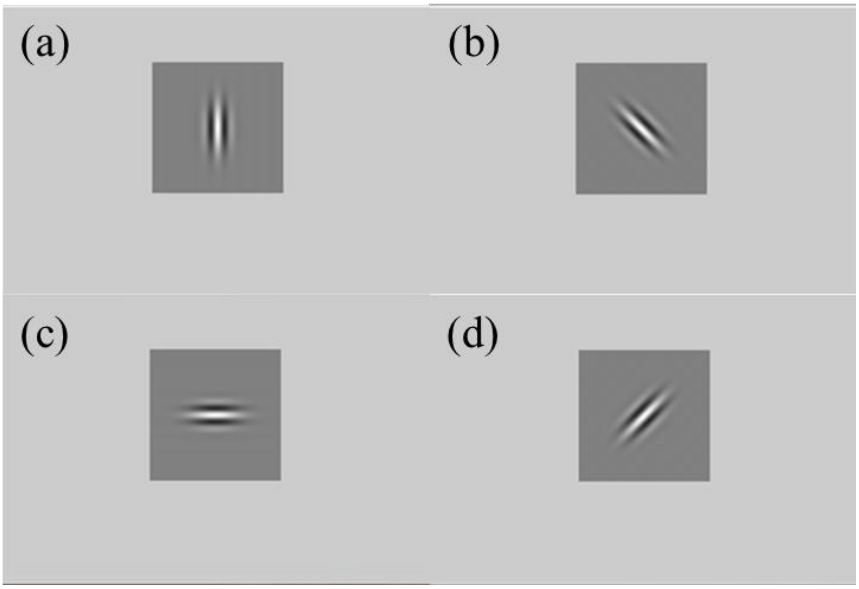

Figure 4.7: The Gabor filters obtained by setting K =1, γ = 0.5, λ = 8, φ = 0 and (a) θ = 0^0, (b) θ = 45^0, (c) θ = 90^0 and (d) θ = 135^0.

4.4 Results and Discussion

The accuracy of the proposed method in locating the bin area and classifying the waste level is evaluated separately. First, the bin area is detected since garbage level classification is only meaningful if the bin is located correctly. The performance of the

proposed method in locating the bin and classifying the level in single bin images are compared against that of the dynamic time warping (DTW) approach used by Islam et Al. [97]. Both methods use an empty bin template, but in the DTW method the template is simply moved in 20 pixel step across the image to find an area that best matches the template. At each location, row and column intensity projection is performed on a 300x300 pixel area to produce a series of values. Then the sequence of projection values is compared with the one obtained from the template using DTW. The location that gives the minimum distance between the two sequences is considered as the true location of the bin. For empty and partially full bin, the classification accuracy of the DTW method is 100% but it drops to 96% and 82% for full and overflowing bin respectively. This is because in some erroneous images the edge and corners of the bin are occluded by rubbish. To achieve good bin localization accuracy, the DTW method requires the bin opening area to be as similar to the template as possible. Thus, the presence of objects that are absent in the templates confuses the DTW algorithm and affects its accuracy. The bin localization accuracy of the proposed method is 100% for empty, partially full and full bins. For overflowing bins the accuracy drops a bit to 99%. The 1% error occurs when the bin opening is almost completely occluded by waste. Samples of detected bin area by DTW and the proposed method are shown in Figure 4.8 while the results are summarized in Table 4.2.

For waste level classification, the DTW method employs a multilayer perceptron (MLP) as a classifier. The method uses both sine and cosine functions at a single orientation to modulate the Gaussian function to produce one Gabor filter. After convolving the bin area with the Gabor filter, it performs column projection on the magnitude of the convolution result to generate 300 feature values. The features are used as inputs to the MLP classifier to determine the waste level of the bin. The classifiers of both methods were trained using 100 images of a garbage bin with

different waste levels. Then their ability to classify the waste level of 200 test images is tested. For each test image, if the bin location is correctly detected then its waste level will be classified. Otherwise, the waste level would not be evaluated since it was irrelevant.

Table 4.2: Performance comparison of the proposed and the DTW methods in bin area detection

Classes	DTW			Proposed Method		
	TP	FN	Accuracy	TP	FN	Accuracy
Empty	50	0	100.00%	50	0	100.00%
Low	0	0	100.00%	0	0	100.00%
Full	48	2	96.00%	50	0	100.00%
Overflow	41	9	82.00%	49	1	98.00%
		Average	94.50%		Average	99.50%

TP = True Positive
FN = False negative

Finally, the classifier of our method was replaced by a K nearest neighbor (KNN) and MLP to see how they fared against SVMs. Table 4.3 summarizes the outcome of the waste level classification and the performances of the different classifiers. It should be noted that only one KNN and MLP classifier was used in the experiments as opposed to three SVMs.

Candidates of the images with three bins also filtered and the features were extracted by Gabor filter. The exact locations of the bins were detected by SVM. The number of locations indicates the number of bins present in the frame. 100 images were selected to train the classifier to detect bin locations. The rest of the images from the dataset (200 images) were used as test image for the classifier. Bin images extracted from the first layer were used in the following layers for level classification. The results

of bin locations detected in the three bin images at different conditions are shown in Figure 4.9 and Figure 4.10.

(a)

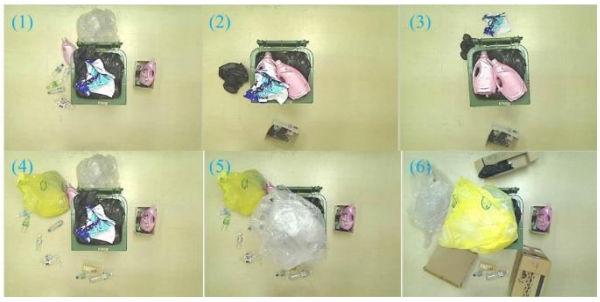

(b)

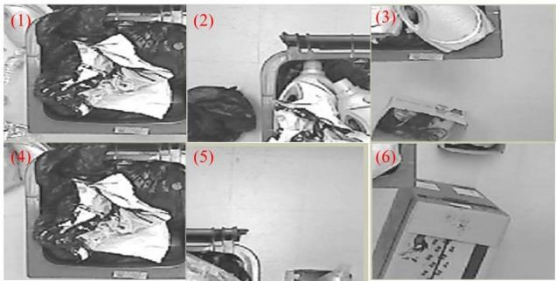

(c)

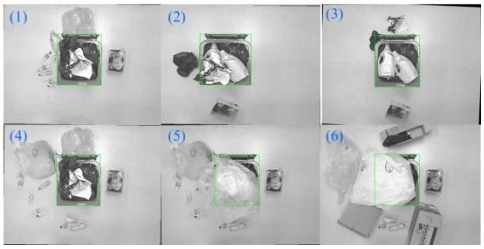

Figure 4.8: Comparison of bin location detection by DTW and proposed method (a) Input images (b) detected bins by DTW and (c) by the proposed method.

Table 4.3: Waste level classification results of the proposed method against the DTW approach

Methods	Bin Detection		Classification		Overall Accuracy	Execution Time
	Total Tested	Correct Number	Classified Total	Number Correct		
DTW-MLP	200	189	189	186	93.00%	2.46s
Proposed Method-KNN	200	199	199	195	98.00%	0.63s
Proposed Method-MLP	200	199	199	196	99.00%	1.13s
Proposed Method-SVM	200	199	199	199	100.00%	0.63s

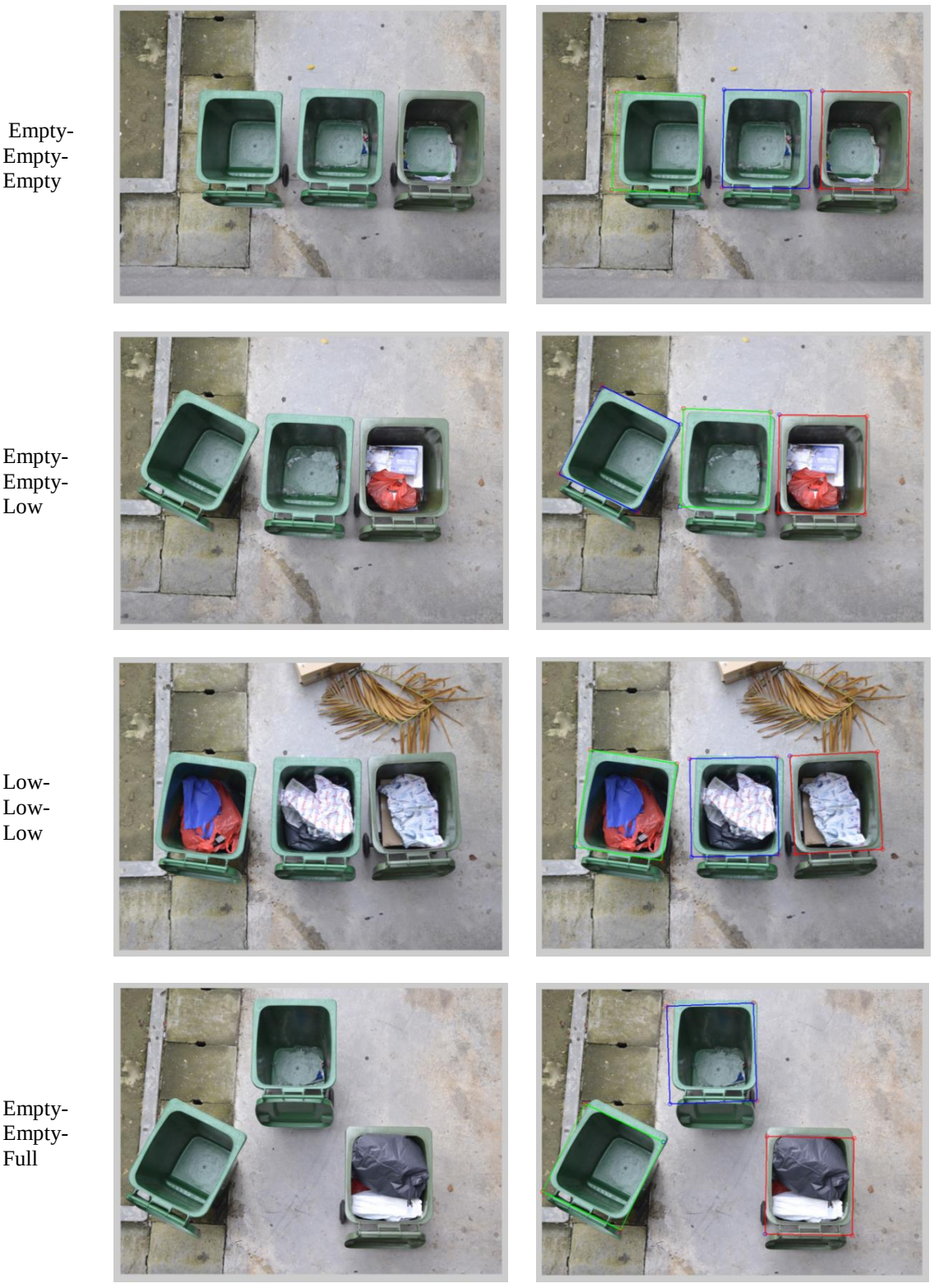

Figure 4.9: Detected bin location in three bin images (a) Level, (b) Input image and (c) Detected locations.

Full-
Low-
Full

Full-
Full
Full

Overflow
-
Overflow
-
Full

Overflow
-
Overflow
-
Toppled

(a) (b) (c)

Figure 4.10: Detected bin location in three bin images (a) Level, (b) Input image and (c) Detected locations.

The conditions of the bins in three bin images were observed by SVM classification of waste level. The output sequence of the classifier was used as the training observation of HMM. The HMM parameters were calculated by Forward-Backward algorithm and optimized by Baum–Welch algorithm. The states are decoded by Viterbi algorithm. Rate of successful estimated states were considered as the score of the model. The model was optimized until the score 100%. The confusion matrix of collection states of the waste bins decoded by HMM is shown in Table 4.4. The average accuracy of the state estimator found 100%.

Table 4.4: Confusion matrix of state estimation

Conditions	Not Necessary	3 days	2 days	1 day	Immediate
Not Necessary	25	0	0	0	0
3 days	0	14	0	0	0
2 days	0	0	10	0	0
1 day	0	0	0	21	0
Immediate	0	0	0	0	30

4.5 Summary

In this chapter the method of second case study about garbage level classification in solid waste bins and the rubbish collection schedule is described elaborately. The system classifies the bin levels using SVM and determines the days left before collection using HMM. The results of the method are compiled in result and discussion section. The results prove that the system is robust against bin shift and rotation, occlusion by large objects and uncertainty introduced by similar square objects littered outside the bin.

CHAPTER 5

Conclusion

5.1 Introduction

The objective of the thesis is showcase two applications of SVM and HMM working in tandem. In the first case study SVM and HMM are used with other signal processing tools navigate a wheel chair in semi-autonomous mode. In the second case study, they are used with other image processing tools to determine the waste level in several bins to decide the collection schedule. The performance of the method is compared with the methods used for those cases in previous works.

5.2 Summary of the Work

In the first case of study, electrooculography (EOG) traces within the electroencephalography (EEG) signals are used to drive a wheelchair navigation system. Sliding window is used to capture important signatures in the EOG traces accurately without partial loss of information. Features are extracted from the signals in the window and used to infer the condition (whether they are open or closed) and gaze direction of the eyes using a number of SVMs and an HMM. The HMM determines the state of the system and generates commands sequentially that move the wheelchair. The wheelchair can be steered in six directions and three different modes of operation are made available to ensure safety and convenience to the user. The asynchronous system achieves an average classification rate of 98% in an online test while its average execution time is less than 1s. An actual navigation session was performed wherein five participants undertook two navigation tasks by maneuvering the wheelchair through two designated routes. The participants managed to complete the tasks without collisions. In this session, the usability of the backward movement proved useful when the wheelchair was trapped at tight dead ends with no space to make u-turn. Good average

accuracy of 98% for Route 1 and 97% for Route 2 shows that the system is easy to use and stable. The second case study introduces a bin detection algorithm that employs Hough line detection and simple cross correlation to detect the position and orientation of a garbage bin in an image. Then Gabor filtering is performed to extract eight features from the inside and outside of the bin area. Together with the number of bin corners detected, the eight Gabor features are used as inputs to four SVM classifiers to determine the waste level in the bin which is either empty, partially, full or overflowing. The outcome of the classifier used in HMM as observation to estimate the collection schedule of solid wastes. The proposed system was tested on a custom database comprising 200 images of single and 100 images of three shifted, rotated, occluded and toppled bin containing garbage of various levels. It achieved an excellent bin detection rate of 99.5%, waste level classification rate of 100% and the combined state estimator of showed a 100% accurate performance on estimating collection states from the waste levels. The method outperforms the dynamic time warping (DTW) approach in both bin detection and waste level classification. The results prove that the system is robust against bin shift and rotation, occlusion by large objects and uncertainty introduced by similar square objects littered outside the bin. Its fast execution time makes it suitable for real time application.

5.3 Future Work

Despite the encouraging results, there are always avenues to enhance the performance and robustness of the method. Since the participants of the wheel chair navigation experiments are all healthy this system still need to be tested by real patients with neuromuscular disordered. The second case study only involves bin with rectangular shape. The robustness of the system should be tested on bins with different shapes, sizes and colors. In future work different kernel functions can be tested to

optimize the classification performance of the SVM. Fuzzy HMM could be implemented to improve the state transition accuracy in future works.

5.4 Points of Summary

The following points are summarized from the thesis

- A method is developed and tested to classify eye gaze movements from EEG and estimate the states using HMM for “Eye Gaze Controlled Automated Wheel Chair Maneuver System Using Brain Controlled Interface”.
- A “Solid Waste Bin Level Classification and Collection Scheduling” method using SVM and HMM is developed and implemented.
- The results of the proposed model are compared with previous methods.

Bibliography

[1] R. C. Ficke, "Digest of Data on Persons with Disabilities," 1992.

[2] C. J. Murray and A. D. Lopez, "Alternative projections of mortality and disability by cause 1990–2020: Global Burden of Disease Study," *The Lancet*, vol. 349, pp. 1498-1504, 1997.

[3] G. T. Carter, *Rehabilitation of Neuromuscular Disease*: WB Saunders, 1998.

[4] L. Y. Deng, C. L. Hsu, T. C. Lin, J. S. Tuan, and S. M. Chang, "EOG-based Human–Computer Interface system development," *Expert Systems with Applications*, vol. 37, pp. 3337-3343, 2010.

[5] R. J. K. Jacob, "The Use of Eye-Movements in Human-Computer Interaction Techniques - What You Look at Is What You Get," *Acm Transactions on Information Systems*, vol. 9, pp. 152-169, Apr 1991.

[6] J. R. Wolpaw, N. Birbaumer, D. J. McFarland, G. Pfurtscheller, and T. M. Vaughan, "Brain–computer interfaces for communication and control," *Clinical neurophysiology*, vol. 113, pp. 767-791, 2002.

[7] J. Jin, E. W. Sellers, and X. Y. Wang, "Targeting an efficient target-to-target interval for P300 speller brain-computer interfaces," *Medical & Biological Engineering & Computing*, vol. 50, pp. 289-296, Mar 2012.

[8] B. Rebsamen, C. T. Guan, H. H. Zhang, C. C. Wang, C. Teo, M. H. Ang, *et al.*, "A Brain Controlled Wheelchair to Navigate in Familiar Environments," *IEEE Transactions on Neural Systems and Rehabilitation Engineering*, vol. 18, pp. 590-598, Dec 2010.

[9] T. Y. Yu, Y. Q. Li, J. Y. Long, and Z. H. Gu, "Surfing the internet with a BCI mouse," *Journal of Neural Engineering*, vol. 9, Jun 2012.

[10] B. Z. Allison, C. Brunner, C. Altstatter, I. C. Wagner, S. Grissmann, and C. Neuper, "A hybrid ERD/SSVEP BCI for continuous simultaneous two dimensional cursor control," *Journal of Neuroscience Methods*, vol. 209, pp. 299-307, Aug 15 2012.

[11] K. B. Ng, A. P. Bradley, and R. Cunnington, "Stimulus specificity of a steady-state visual-evoked potential-based brain-computer interface," *Journal of Neural Engineering*, vol. 9, Jun 2012.

[12] H. J. Hwang, J. H. Lim, Y. J. Jung, H. Choi, S. W. Lee, and C. H. Im, "Development of an SSVEP-based BCI spelling system adopting a QWERTY-style LED keyboard," *Journal of Neuroscience Methods*, vol. 208, pp. 59-65, Jun 30 2012.

[13] T. O. Zander, M. Gaertner, C. Kothe, and R. Vilimek, "Combining eye gaze input with a brain–computer interface for touchless human–computer interaction," *Intl. Journal of Human–Computer Interaction*, vol. 27, pp. 38-51, 2010.

[14] M. Fatourechi, A. Bashashati, R. K. Ward, and G. E. Birch, "EMG and EOG artifacts in brain computer interface systems: A survey," *Clin Neurophysiol,* vol. 118, pp. 480-94, Mar 2007.

[15] F. Lotte, M. Congedo, A. Lecuyer, F. Lamarche, and B. Arnaldi, "A review of classification algorithms for EEG-based brain-computer interfaces," *J Neural Eng,* vol. 4, pp. R1-R13, Jun 2007.

[16] Z. Minghua, F. Xiumin, A. Rovetta, H. Qichang, F. Vicentini, L. Bingkai, *et al.*, "Municipal solid waste management in Pudong New Area, China," *Waste management,* vol. 29, pp. 1227-1233, 2009.

[17] L. A. Guerrero, G. Maas, and W. Hogland, "Solid waste management challenges for cities in developing countries," *Waste management,* vol. 33, pp. 220-232, 2013.

[18] A. Scheinberg, D. Wilson, and L. Rodic, "Solid waste management in the world's cities," *UN-Habitat's State of Water and Sanitation in the World's Cities Series, Earthscan for UN-Habitat, London and Washington DC,* 2010.

[19] A. Scheinberg, *Value added: modes of sustainable recycling in the modernisation of waste management systems*: publisher not identified, 2011.

[20] L. A. Wright, J. Coello, S. Kemp, and I. Williams, "Carbon footprinting for climate change management in cities," *Carbon Management,* vol. 2, pp. 49-60, 2011.

[21] M. Arebey, M. Hannan, H. Basri, R. Begum, and H. Abdullah, "Solid waste monitoring system integration based on RFID, GPS and camera," in *Intelligent and Advanced Systems (ICIAS), 2010 International Conference on*, 2010, pp. 1-5.

[22] O. M. Johansson, "The effect of dynamic scheduling and routing in a solid waste management system," *Waste management,* vol. 26, pp. 875-885, 2006.

[23] L. R. Rabiner, "A Tutorial on Hidden Markov-Models and Selected Applications in Speech Recognition," *Proceedings of the IEEE,* vol. 77, pp. 257-286, Feb 1989.

[24] L. E. Baum, "An equality and associated maximization technique in statistical estimation for probabilistic functions of Markov processes," *Inequalities,* vol. 3, pp. 1-8, 1972.

[25] L. E. Baum, T. Petrie, G. Soules, and N. Weiss, "A maximization technique occurring in the statistical analysis of probabilistic functions of Markov chains," *The annals of mathematical statistics,* pp. 164-171, 1970.

[26] A. J. Viterbi, "Error bounds for convolutional codes and an asymptotically optimum decoding algorithm," *Information Theory, IEEE Transactions on,* vol. 13, pp. 260-269, 1967.

[27] G. D. Forney Jr, "The viterbi algorithm," *Proceedings of the IEEE,* vol. 61, pp. 268-278, 1973.

[28] D. Kumar, A. Sachan, and M. Kumar, "Implementation of Speech Recognition in Web Application for Sub Continental Language."

[29] J. Xin and Y. Qi, "Speech Recognition," in *Mathematical Modeling and Signal Processing in Speech and Hearing Sciences*, ed: Springer, 2014, pp. 115-139.

[30] A. Cassese, M. Guindani, M. G. Tadesse, F. Falciani, and M. Vannucci, "A hierarchical Bayesian model for inference of copy number variants and their association to gene expression," *The Annals of Applied Statistics*, vol. 8, pp. 148-175, 2014.

[31] S. Fine, Y. Singer, and N. Tishby, "The hierarchical hidden Markov model: Analysis and applications," *Machine learning*, vol. 32, pp. 41-62, 1998.

[32] N. N. Jetha, "Advances in nanopore sensing for DNA and protein analysis," 2014.

[33] J. Møller and R. D. Jacobsen, "Gaussian-log-Gaussian wavelet trees, frequentist and Bayesian inference, and statistical signal processing applications," 2014.

[34] Y. Morere, A. Pruski, and A. C. Malti, "Aided navigation for disabled people: route recognition," in *Systems, Man and Cybernetics, 2002 IEEE International Conference on*, 2002, p. 5 pp. vol.4.

[35] Y. Morère and A. Pruski, "A multi-agent control structure for intelligent wheelchair and Aided navigation for disabled people," in *Proceedings of the 2004 International Symposium on Robotics (ISR 2004)*, 2004, pp. 23-26.

[36] M. Ren and H. A. Karimi, "A hidden Markov model-based map-matching algorithm for wheelchair navigation," *Journal of Navigation*, vol. 62, pp. 383-395, 2009.

[37] C. Bartolein, A. Wagner, M. Jipp, and E. Badreddin, "Easing wheelchair control by gaze-based estimation of intended motion," in *Proceedings of the IFAC World Congress*, 2008, pp. 9162-9167.

[38] C. Anand and R. Lawrance, "Seven State HMM-Based Face Recognition System along with SVD Coefficients," *Biometrics and Bioinformatics*, vol. 5, pp. 226-233, 2013.

[39] O. Samanta, U. Bhattacharya, and S. Parui, "Smoothing of HMM Parameters for Efficient Recognition of Online Handwriting," *Pattern Recognition*, 2014.

[40] S. Vishwanathan and M. Narasimha Murty, "SSVM: a simple SVM algorithm," in *Neural Networks, 2002. IJCNN'02. Proceedings of the 2002 International Joint Conference on*, 2002, pp. 2393-2398.

[41] L. Zhiwei and S. Minfen, "Classification of mental task EEG signals using wavelet packet entropy and SVM," in *Electronic Measurement and Instruments, 2007. ICEMI'07. 8th International Conference on*, 2007, pp. 3-906-3-909.

[42] N. Cristianini and J. Shawe-Taylor, *An introduction to support vector machines and other kernel-based learning methods*: Cambridge university press, 2000.

[43] B. Schölkopf and A. J. Smola, *Learning with kernels*: “The” MIT Press, 2002.

[44] M. J. E. S. A. Khorshidtalab, "EEG signal classification for real-time brain-computer interface applications: A review," presented at the Mechatronics (ICOM), 2011 4th International Conference, Kuala Lumpur, 2011.

[45] F. M. d. S. Matos and R. M. C. R. de Souza, "Vehicle Image Classification Method Using Edge Dimensions, SVM and Prototype."

[46] O. Chapelle, P. Haffner, and V. N. Vapnik, "Support vector machines for histogram-based image classification," *Neural Networks, IEEE Transactions on,* vol. 10, pp. 1055-1064, 1999.

[47] M. Nakajima, C. Yen-Wei, and H. Xian-Hua, "Adaptive color discrimination for image classification," in *Biomedical Engineering and Informatics (BMEI), 2013 6th International Conference on*, 2013, pp. 826-830.

[48] H. Xu, W. Song, Z. Hu, C. Chen, X. Zhao, and J. Zhang, "A speedup SVM decision method for online EEG processing in motor imagery BCI," in *Intelligent Systems Design and Applications (ISDA), 2010 10th International Conference on*, 2010, pp. 149-153.

[49] Y.-P. Lin, C.-H. Wang, T.-L. Wu, S.-K. Jeng, and J.-H. Chen, "Support vector machine for EEG signal classification during listening to emotional music," in *Multimedia Signal Processing, 2008 IEEE 10th Workshop on*, 2008, pp. 127-130.

[50] B. Rebsamen, E. Burdet, G. Cuntai, Z. Haihong, T. Chee Leong, Q. Zeng, *et al.*, "A Brain-Controlled Wheelchair Based on P300 and Path Guidance," in *Biomedical Robotics and Biomechatronics, 2006. BioRob 2006. The First IEEE/RAS-EMBS International Conference on*, 2006, pp. 1101-1106.

[51] Y. Jianchao, Y. Kai, G. Yihong, and T. Huang, "Linear spatial pyramid matching using sparse coding for image classification," in *Computer Vision and Pattern Recognition, 2009. CVPR 2009. IEEE Conference on*, 2009, pp. 1794-1801.

[52] S. Belongie, J. Malik, and J. Puzicha, "Shape matching and object recognition using shape contexts," *Pattern Analysis and Machine Intelligence, IEEE Transactions on,* vol. 24, pp. 509-522, 2002.

[53] J. Canny, "A Computational Approach to Edge Detection," *Pattern Analysis and Machine Intelligence, IEEE Transactions on,* vol. PAMI-8, pp. 679-698, 1986.

[54] J. B. Ochoa, "EEG signal classification for brain computer interface applications," *Ecole Polytechnique Federale De Lausanne,* 2002.

[55] T. J. Sullivan, S. R. Deiss, J. Tzyy-Ping, and G. Cauwenberghs, "A brain-machine interface using dry-contact, low-noise EEG sensors," in *Circuits and Systems, 2008. ISCAS 2008. IEEE International Symposium on*, 2008, pp. 1986-1989.

[56] J. Löfhede, F. Seoane, and M. Thordstein, "Textile Electrodes for EEG Recording — A Pilot Study," *Sensors,* vol. 12, pp. 16907-16919, 2012.

[57] J. Gomez-Gil, I. San-Jose-Gonzalez, L. F. Nicolas-Alonso, and S. Alonso-Garcia, "Steering a tractor by means of an EMG-based human-machine interface," *Sensors (Basel)*, vol. 11, pp. 7110-26, 2011.

[58] J. Malmivuo and R. Plonsey, *Bioelectromagnetism: principles and applications of bioelectric and biomagnetic fields*. New York, USA: Oxford University Press, 1995.

[59] L. P. Rowland and N. A. Shneider, "Amyotrophic Lateral Sclerosis," *New England Journal of Medicine*, vol. 344, pp. 1688-1700, 2001.

[60] A. E. H. Emery, "Population frequencies of inherited neuromuscular diseases—A world survey," *Neuromuscular Disorders*, vol. 1, pp. 19-29, 1991.

[61] C. Coers, N. Telerman-Toppet, and J.-M. Gerard, "Terminal innervation ratio in neuromuscular disease: II. Disorders of lower motor neuron, peripheral nerve, and muscle," *Archives of Neurology*, vol. 29, p. 215, 1973.

[62] R. T. Abresch, G. T. Carter, M. P. Jensen, and D. D. Kilmer, "Assessment of pain and health-related quality of life in slowly progressive neuromuscular disease," *American Journal of Hospice and Palliative Medicine*, vol. 19, pp. 39-48, 2002.

[63] S. P. Levine, D. A. Bell, L. A. Jaros, R. C. Simpson, Y. Koren, and J. Borenstein, "The NavChair assistive wheelchair navigation system," *Rehabilitation Engineering, IEEE Transactions on*, vol. 7, pp. 443-451, 1999.

[64] R. C. Simpson and S. P. Levine, "Automatic adaptation in the NavChair assistive wheelchair navigation system," *Rehabilitation Engineering, IEEE Transactions on*, vol. 7, pp. 452-463, 1999.

[65] T. Röfer and A. Lankenau, "Architecture and applications of the Bremen Autonomous Wheelchair," *Information Sciences*, vol. 126, pp. 1-20, 2000.

[66] N. I. Katevas, N. Sgouros, S. Tzafestas, G. Papakonstantinou, P. Beattie, J. Bishop, *et al.*, "The autonomous mobile robot SENARIO: a sensor aided intelligent navigation system for powered wheelchairs," *Robotics & Automation Magazine, IEEE*, vol. 4, pp. 60-70, 1997.

[67] H. Hoyer, R. Hoelper, U. Borgolte, C. Bühler, H. Heck, W. Humann, *et al.*, "The omni wheelchair with high manoeuvrability and navigational intelligence," in *Rehabilitation Technology, Proc. of the 2nd TIDE Congress, Brussels, IOS Press*, 1995.

[68] E. Prassler, J. Scholz, and P. Fiorini, "A robotics wheelchair for crowded public environment," *Robotics & Automation Magazine, IEEE*, vol. 8, pp. 38-45, 2001.

[69] H. A. Yanco, "Wheelesley: A robotic wheelchair system: Indoor navigation and user interface," in *Assistive technology and artificial intelligence*, ed: Springer, 1998, pp. 256-268.

[70] G. Bourhis and Y. Agostini, "The VAHM robotized wheelchair: System architecture and human-machine interaction," *Journal of Intelligent and Robotic Systems*, vol. 22, pp. 39-50, 1998.

[71] J. Millán, F. Galán, D. Vanhooydonck, E. Lew, J. Philips, and M. Nuttin, "Asynchronous non-invasive brain-actuated control of an intelligent wheelchair," in *Engineering in Medicine and Biology Society, 2009. EMBC 2009. Annual International Conference of the IEEE*, 2009, pp. 3361-3364.

[72] B. Rebsamen, E. Burdet, C. Guan, H. Zhang, C. L. Teo, Q. Zeng, *et al.*, "A brain-controlled wheelchair based on P300 and path guidance," in *Biomedical Robotics and Biomechatronics, 2006. BioRob 2006. The First IEEE/RAS-EMBS International Conference on*, 2006, pp. 1101-1106.

[73] R. Barea, L. Boquete, L. M. Bergasa, E. Lopez, and M. Mazo, "Electro-oculographic guidance of a wheelchair using eye movements codification," *International Journal of Robotics Research,* vol. 22, pp. 641-652, Jul-Aug 2003.

[74] J. d. R. Millán, R. Rupp, G. R. Müller-Putz, R. Murray-Smith, C. Giugliemma, M. Tangermann, *et al.*, "Combining brain–computer interfaces and assistive technologies: state-of-the-art and challenges," *Frontiers in neuroscience,* vol. 4, 2010.

[75] (25th October). *PeopleBot*. Available: http://www.mobilerobots.com/researchrobots/peoplebot.aspx

[76] (25 October). *iRobot*. Available: http://www.irobot.com/us/

[77] (25 October). *Robotino*. Available: http://www.festo.com/cms/en_corp/11367.htm

[78] J. R. Millan, F. Renkens, J. Mouriño, and W. Gerstner, "Noninvasive brain-actuated control of a mobile robot by human EEG," *Biomedical Engineering, IEEE Transactions on*, vol. 51, pp. 1026-1033, 2004.

[79] R. Barea, L. Boquete, M. Mazo, and E. Lopez, "System for assisted mobility using eye movements based on electrooculography," *IEEE Trans Neural Syst Rehabil Eng,* vol. 10, pp. 209-18, Dec 2002.

[80] R. Barea, L. Boquete, S. Ortega, E. López, and J. M. Rodríguez-Ascariz, "EOG-based eye movements codification for human computer interaction," *Expert Systems with Applications,* vol. 39, pp. 2677-2683, Feb 15 2012.

[81] J. Gips and P. Olivieri, "EagleEyes: An eye control system for persons with disabilities," *online] http://www. cs. bc. edu/~ eagleeye/papers/paper1/paper1. html viewed,* vol. 10, p. 05, 1996.

[82] T. E. Hutchinson, K. P. White, W. N. Martin, K. C. Reichert, and L. A. Frey, "Human-Computer Interaction Using Eye-Gaze Input," *Ieee Transactions on Systems Man and Cybernetics,* vol. 19, pp. 1527-1534, Nov-Dec 1989.

[83] Q. Ji and X. Yang, "Real-time eye, gaze, and face pose tracking for monitoring driver vigilance," *Real-Time Imaging,* vol. 8, pp. 357-377, 2002.

[84] R. Barea, L. Boquete, M. Mazo, and E. López, "Wheelchair guidance strategies using EOG," *Journal of intelligent and robotic systems,* vol. 34, pp. 279-299, 2002.

[85] S. Yathunanthan, L. Chandrasena, A. Umakanthan, V. Vasuki, and S. Munasinghe, "Controlling a wheelchair by use of EOG signal," in *Information and Automation for Sustainability, 2008. ICIAFS 2008. 4th International Conference on*, 2008, pp. 283-288.

[86] W. S. Wijesoma, K. S. Wee, O. C. Wee, A. P. Balasuriya, K. T. San, and L. K. Soon, "EOG based control of mobile assistive platforms for the severely disabled," in *Robotics and Biomimetics (ROBIO). 2005 IEEE International Conference on*, 2005, pp. 490-494.

[87] B. Champaty, J. Jose, K. Pal, and A. Thirugnanam, "Development of EOG based human machine interface control system for motorized wheelchair," in *Emerging Research Areas: Magnetics, Machines and Drives (AICERA/iCMMD), 2014 Annual International Conference on*, 2014, pp. 1-7.

[88] R. Barea, L. Boquete, M. Mazo, E. López, and L. M. Bergasa, "EOG guidance of a wheelchair using neural networks," in *Pattern Recognition, 2000. Proceedings. 15th International Conference on*, 2000, pp. 668-671.

[89] M. Noor, N. Muthmainnah, and S. Ahmad, "Implementation of Fuzzy Logic Controller for Wheelchair Motion Control Based on EOG Data," in *Applied Mechanics and Materials*, 2014, pp. 183-189.

[90] M. Hashimoto, K. Takahashi, and M. Shimada, "Wheelchair control using an EOG-and EMG-based gesture interface," in *Advanced Intelligent Mechatronics, 2009. AIM 2009. IEEE/ASME International Conference on*, 2009, pp. 1212-1217.

[91] L. Wei, H. Hu, and K. Yuan, "Use of forehead bio-signals for controlling an intelligent wheelchair," in *Robotics and Biomimetics, 2008. ROBIO 2008. IEEE International Conference on*, 2009, pp. 108-113.

[92] A. Fuchs, H. Zangl, G. Holler, and G. Brasseur, "Design and analysis of a capacitive moisture sensor for municipal solid waste," *Measurement Science and Technology*, vol. 19, p. 025201, 2008.

[93] F. Reverter, M. Gasulla, and R. Pallas-Areny, "Capacitive level sensing for solid-waste collection," in *Sensors, 2003. Proceedings of IEEE*, 2003, pp. 7-11.

[94] M. J. B. Marques, "Reliability Of A Line-of-view Sensor For Recycling Point Waste Containers."

[95] C. Marzano, F. Fratello, F. Moroni, M. C. Pellicciari, G. Curcio, M. Ferrara, *et al.*, "Slow eye movements and subjective estimates of sleepiness predict EEG power changes during sleep deprivation," *SLEEP-NEW YORK THEN WESTCHESTER-*, vol. 30, p. 610, 2007.

[96] J. G. Daugman, "Uncertainty relation for resolution in space, spatial frequency, and orientation optimized by two-dimensional visual cortical filters," *JOSA A*, vol. 2, pp. 1160-1169, 1985.

[97] M. S. Islam, M. Hannan, H. Basri, A. Hussain, and M. Arebey, "Solid waste bin detection and classification using Dynamic Time Warping and MLP classifier," *Waste management*, vol. 34, pp. 281-290, 2014.

Appendix A

Gray Level Aura Matrix

The GLAM of an image measures the amount of each gray level in the neighborhood of each other gray level. An example of an aura on a binary lattice with the four nearest neighborhood system is shown in figure. The aura ‘c’ of ‘a’ with respect to ‘b’ characterizes how the subset ‘b’ is present in the neighborhood of ‘a’. The aura measure m(a, b) measures the amount of ‘b’s sites presented in the neighborhood of ‘a’.

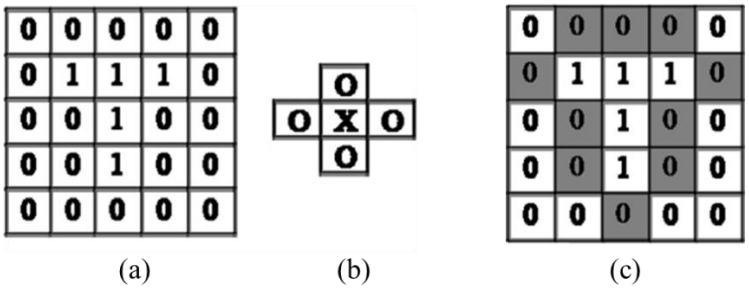

Figure: Example of an aura matrix on a binary lattice with the four-NS.

Appendix B

K nearest Neighbor

The KNN algorithm is considered as supervised learning method used in image processing applications. Samples are classified based on closest training by a majority vote of its neighbors (Maji & Pal, 2010). The feature vectors are stored in the training period. The class of the test sample K is determined by the distances from the sample to the train vectors. The Euclidean distance is measured by examining the root of square differences between the coordinates of two samples. The minimum distance from vectors belong to a specific class indicate the presence of nearest neighbors feature vectors of that class around the K. In Figure the mapping of the K-vector and features on a 2 dimensional space are shown. d_c are the distance from the K to c class vectors, “*”,

“x” and “o” are the training vector from different classes and • is the K vector for testing.

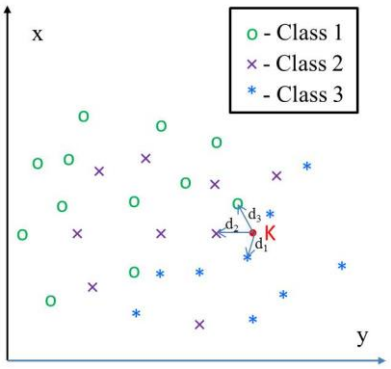

Figure : Map of KNN classifier

Appendix C

Neural Network

Artificial neural networks (NNs) which are inspired by biological nervous systems are promising and powerful tools in identification and modeling of nonlinear systems due to their impressive merit in data processing and learning capabilities. As the name Multilayer Neural Networks suggests, the network consists of multiple layers of neurons which are usually considered as three layers, namely input layer, hidden layer and output layer. However, the number of neurons in each layer is to be determined and can be defined based on the designer choice. Figure shows a three layer neural network where the two weighting matrices, W and V are depicted by arrows.

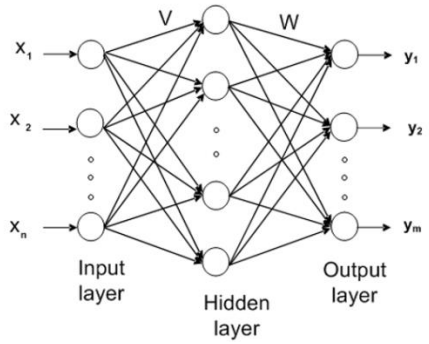

Figure : Basic Schematic of Neural network

The real capability of multilayer NNs is due to their ability in approximating nonlinear functions. The Cybenko theorem [39] shows that a feed forward neural network is capable of approximating any continuous, multivariate function to any desired degree of accuracy. Nonlinear parameter selections of neural network showed robust performance for flexible joint state estimation in a robotic simulation by Abdollahi, Farazaneh et al, (Abdollahi, Talebi, & Patel, 2006). The combined state estimation using neural network and Kalman filter provide an easier and improved algorithm for approximation problems ("Frontmatter and Index," 2002; Iiguni, Sakai, & Tokumaru, 1992). The limitation of any neural network to map a function arises from poor selection of the neural network parameters and weights or an insufficient number of the hidden neurons.

Appendix D

Dynamic Time warping

DTW algorithm has grossed its acceptance by being very efficient to detect pattern similarity. It minimizes the distortion and shifting effects by permitting elastic transformation of time series (Assecondi et al., 2009). Suppose U and V are two time series; where, n and m are the respective length. A warping path P is a contiguous set of matrix elements that defines a mapping between Q and C. This path derived from the Euclidian Distance matrixes between each element of the both series. A graphical

representation of the wrapping path has shown in figure. The wrapping path is a set of points from the matrix that follows the minimum distance of adjacent cells. The selection of path value follows three conditions

- **Boundary conditions:** $P_1 = (1,1)$ and $P_K = (m,n)$, simply stated, this requires the warping path to start and finish in diagonally opposite corner cells of the matrix.
- **Continuity:** Given $P_k = (a,b)$ then $P_{k-1} = (a',b')$ where $a–a' \leq 1$ and $b\text{-}b' \leq 1$. This restricts the allowable steps in the warping path to adjacent cells (including diagonally adjacent cells).
- **Monotonicity:** Given $P_k = (a,b)$ then $P_{k-1} = (a',b')$ where $a–a' \geq 0$ and $b\text{-}b' \geq 0$. This forces the points in P to be monotonically spaced in time.

There can be more than one path in the distance matrices that satisfy above conditions. The cost function in (8) defines the scores of the paths.

$$DTW(U,V) = \min\left\{\sqrt{\sum_1^K P_k / K}\right. \tag{8}$$

The wrapping path is the path that minimizes the cost. The cost of the minimum path is considered to be the score of the matching.

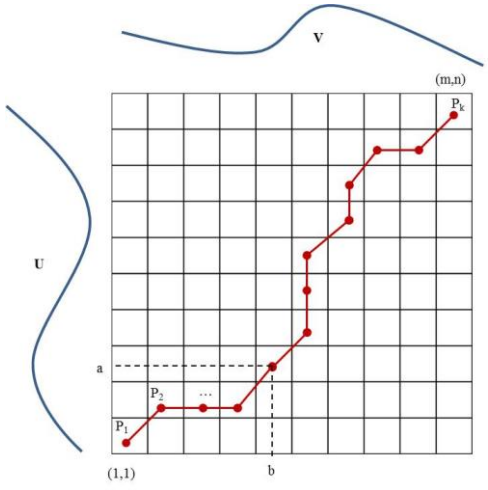

Figure: An Example of Wrapping path

Appendix E

Publications

Fayeem Aziz, Hamzah Arof , Norrima Mokhtar , Marizan Mubin, "HMM based automated wheelchair navigation using EOG traces in EEG ",Journal of Neural Engineering, 2014. 11(5): p. 056018. (ISI Index = Q1)

Fayeem Aziz, Norrima Mokhtar, Hamzah Arof, Marizan Mubin, Zuwairie Ibrahim, "Review of Eye Gaze Tracking Application", The 6th AUN/SEED-Net Regional Conference on Electrical Engineering 2014 4 – 5 March 2014, University of Malaya, 50603 Kuala Lumpur, Malaya. (Presented)